Title

COLLECTIVE EXCITATION OF NEUTRON-DEFICIENT BARIUM, XENON, AND CERIUM ISOTOPES: CENTRIFUGAL STRETCHING TREATMENT OF NUCLEI

Author

Clarkson, Jack E.

Publication Date

1965-05-01

UCRL-16040

University of California

Ernest O. Lawrence Radiation Laboratory

COLLECTIVE EXCITATION OF NEUTRON-DEFICIENT BARIUM, XENON, AND CERIUM ISOTOPES: CENTRIFUGAL STRETCHING TREATMENT OF NUCLEI

Berkeley, California

DISCLAIMER

UCRL-16040

UNIVERSITY OF CALIFORNIA

Lawrence Radiation Laboratory
Berkeley, California

AEC Contract No. W-7405-eng-48

COLLECTIVE EXCITATION OF NEUTRON-DEFICIENT BARIUM, XENON, AND CERIUM ISOTOPES: CENTRIFUGAL STRETCHING TREATMENT OF NUCLEI

Jack E. Clarkson

(Ph.D. Thesis)

May 1965

COLLECTIVE EXCITATION OF NEUTRON-DEFICIENT BARIUM, XENON, AND CERIUM ISOTOPES: CENTRIFUGAL STRETCHING TREATMENT OF NUCLEI

Contents

COLLECTIVE EXCITATION OF NEUTRON-DEFICIENT BARIUM, XENON, AND CERIUM ISOTOPES: CENTRIFUGAL STRETCHING TREATMENT OF NUCLEI

Jack E. Clarkson

Lawrence Radiation Laboratory and Department of Chemistry
University of California
Berkeley, California

May 1965

ABSTRACT

The collective excitation of various neutron-deficient barium, xenon, and cerium isotopes by the "in-beam" method using lithium-drifted germanium counters has been obtained. The (heavy ion, xn) reaction has been used to produce Ba^{126}, Ba^{124}, Xe^{122}, Xe^{120}, and Ce^{134}. The decay of Pr^{134} to Ce^{134} was also observed, with a half-life of 17 ± 2 minutes. Partial level schemes for the ground-state rotational bands to spin 8^+ or 10^+ are proposed for the nuclides investigated. The lifetime of the first-excited state in Ba^{126} has been determined as an "in-beam" experiment to be $2.7 \pm 0.5 \times 10^{-10}$ seconds and, hence, gives the deformation of Ba^{126} as $\beta = 0.24 \pm 0.02$.

The implications of the rotational energies and spacings as related to deformation in this region are discussed.

A classical centrifugal stretching treatment employing realistic nuclear potentials is developed and the results of this and other works are compared to the calculated energy levels from this treatment.

I. INTRODUCTION

The existence of three regions of deformed nuclei is now well established. The properties of these nuclei have been surveyed by several authors.[1,2] The success of the collective model of Bohr and Mottelson[3] has added considerable interest to the study of nuclear levels in these regions, but no model has yet completely described these nuclei. A recent survey of the collective model theories, especially those concerned with the hydrodynamic model of vibrations and rotations of deformed liquid drops was presented by Davidson.[4]

Experimental evidence concerning the region of deformation where N and Z vary from 50 to 82 was first given by Sheline, Sikkeland, and Chanda[5] who observed the first-excited states in Ba^{130}, Ba^{128}, and Ba^{126}. These isotopes were subsequently studied by Chanda,[6,7] who investigated the gamma-gamma coincidence spectrum of the nuclei involved, and proposed partial-level schemes for the three barium nuclei. The evidence suggesting the deformed area of nuclei consisted mainly in (1) systematics of the first-excited state energies, and (2) the ratio of the energy levels observed in relation to that expected for rotational bands in even-even deformed nuclei.

The study of the collective properties of nuclei in this new region of deformation is also the subject of the present work; in particular the collective excitation of Ba^{126}, Ba^{124}, Xe^{122}, Xe^{120}, and Ce^{134}. Since the study of the energy levels of nuclei which are produced by radioactive decay is strongly influenced by the spin of the parent nuclei,

the investigation of collective levels by this technique is limited. Other methods, therefore, were used in most of this work.

Several groups have observed gamma rays emitted from nuclei which were de-exciting after being produced in nuclear reactions. Morinaga and Gugelot[8] first observed the gamma rays in the cascade to lower excited states of nuclei produced in (α, xn) reactions. Hansen, Elbek, Hagemann, and Hornyak[9] used (p, xn) reactions and studied the spectra of the conversion electrons from various targets using a magnetic spectrometer. Stephens, Lark, and Diamond,[10] using (heavy ion, xn) reactions, observed the de-excitation cascades using an electron spectrometer and also NaI(Tl) and germanium solid-state detectors. As shown in these works, the ground-state rotational band could be seen up to the 10+ level, and in some of the cases of Stephens et al. to the 18+ level.

More recently several authors[11-13] have reported studies using similar techniques. The work of Miyano et al. in observing the collective states in Ba^{130} is of particular interest as it is in the neighborhood of the new region of deformation. This work verifies the work of Chanda[6] who used radiochemical techniques on La^{130} to obtain the states in Ba^{130}. The Miyano work also demonstrates the desirability of investigating more of the nuclei in this region with the "in-beam" technique.

The Berkeley heavy-ion linear accelerator (Hilac) was used to produce the isotopes investigated in the present work and the de-excitation of the ground-state rotational bands was observed by use of lithium-drifted germanium counters. Ce^{134} was also studied by the production of Pr^{134}

and observing the radioactive decay after chemical separation. By using an electrostatic method for recoil measurement of nuclear lifetimes developed by Novakov, Hollander, and Graham,[14] the lifetime of the first-excited state of Ba^{126} was observed as an "in-beam" experiment.

In the second part of this work, the results of these studies, along with those of Stephens, Lark, and Diamond[10] will be compared to the rotational spacings calculated from a classical treatment of centrifugal stretching of nuclei.

II. EXPERIMENTAL PROCEDURES

A. Bombardment Methods

The Berkeley heavy-ion linear accelerator (Hilac) was used to accelerate beams of N^{14}, C^{12}, B^{11}, and B^{10} to the energies required to produce Ba^{126}, Ba^{124}, Xe^{122}, Xe^{120}, Ce^{134}, and Pr^{134} from the appropriate targets (Table I). The desired isotope's excitation function was calculated by using the Jackson Model.[15] The ion energy corresponding to the peak in the excitation function was used as a starting point to look for the desired product. A crude excitation function was then experimentally obtained by observing the products at various energies. In most cases the Jackson Model calculated value and the experimental peak value were within ± 3 MeV. The bombarding energy given in Table I is the one which seemed to give predominantly the desired reaction product. In the case of Ba^{124} and Xe^{122}, two different reactions were employed, using different projectiles and targets.

1. "In-Beam" Bombardment Methods

The experimental setup for the "in-beam" gamma-ray detection (Fig. 1) consisted of: (a) a retractable gold scatter foil and a beam-energy detector for beam-energy measurements, (b) a lead collimator of approximately 3/8-in. diameter connected to an electrometer which measured the beam hitting the collimator and facilitated focusing of the beam, (c) the target assembly which included the target on a retractable paddle and lucite windows which allowed viewing the target while in the beam location, (d) the Faraday cup, connected to an electrometer which measured

Table I. Nuclear reactions employed.

Isotope	Reaction	Approx. Heavy Ion Bombarding Energy (MeV)
Ba^{126}	$In^{115}(N^{14}, 3n)Ba^{126}$	52
Ba^{124}	$In^{115}(N^{14}, 5n)Ba^{124}$	84
	$Sn^{116}(C^{12}, 4n)Ba^{124}$	80
Xe^{122}	$In^{115}(B^{10}, 3n)Xe^{122}$	37
	$In^{115}(B^{11}, 4n)Xe^{122}$	57
Xe^{120}	$In^{115}(B^{10}, 5n)Xe^{120}$	67
Ce^{134}	$I^{127}(B^{11}, 4n)Ce^{134}$	57
Pr^{134}	$I^{127}(C^{12}, 5n)Pr^{134}$	90

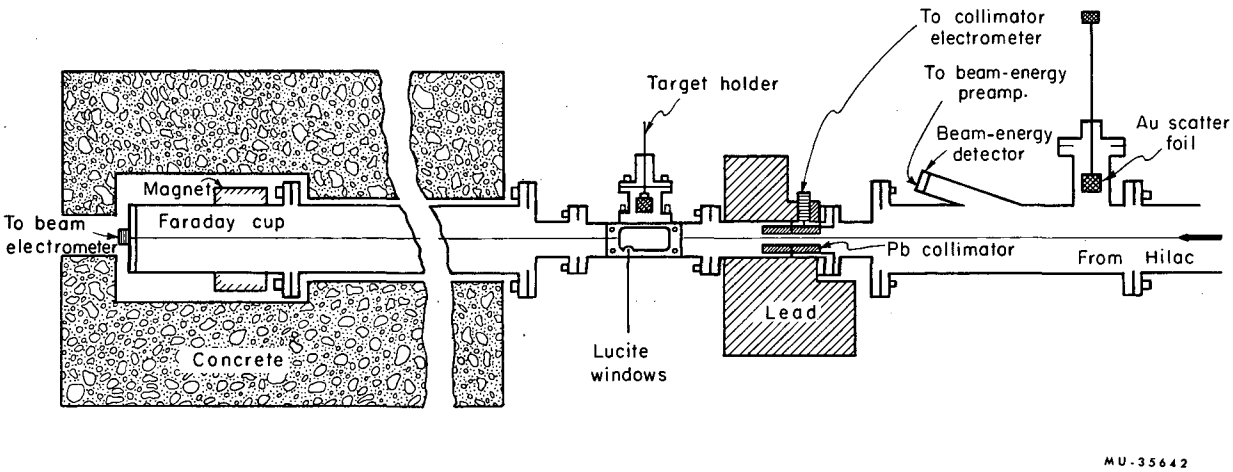

Fig. 1. Vertical cross-section of the experimental setup for gamma-ray detection.

the beam intensity, and (e) the lithium-drifted germanium counter, shown in the instrumental section, IIB.

Since the Hilac "partial-energy" beam was used, no degradation of the beam by absorbers was necessary. The desired energy was achieved by changing the tilt of the gradient in the post-stripper tank, and adjusting the tank tuners to obtain the beam of the desired energy. The beam was magnetically analyzed by deflection through 52°, and then traveled through a quadrupole focusing magnet and into the experimental area. (This entire process was operated by the Hilac crew, generally with little trouble.)

The beam-energy was measured by scattering the beam from a thin ($\sim$ 1 mg/cm^2) gold foil into a solid-state detector which was at an angle of 20° to the beam. The detector was calibrated with the full-energy beam (10.4 $\pm$ 0.2) MeV/nucleon^{16} and the beam energy measured was considered accurate to within 1-2%.

The ratio of the beam hitting the Faraday cup and the beam hitting the collimator in front of the target was used as an aid in final focusing of the beam. This ratio was generally 2:1 or better; although it did at times go as low as 1:2.

The average beam currents were held to a few mμA when using the Li-drifted germanium counter to detect the gamma rays. The beam-pulse repetition rate was twelve pulses per second in the earlier part of this work, and was later increased to forty pulses per second due to modifications made at the Hilac. The beam-pulse length was $\sim$ 3 milliseconds.

The targets used were of two types: (1) thin self-supporting targets, and (2) thick targets. Thin self-supporting targets of indium and separated tin isotope were used in the gamma-ray apparatus as previously described (see also Fig. 1). Thick targets of indium and lead iodide were used in a terminating target holder, where the target holder was itself used as the Faraday cup.

The thick targets were: 0.003-in. thick indium foil targets, and approximately 20 mg/cm^2 lead iodide powder which served as an iodine target. The lead iodide target was made by pressing the powdered lead iodide into a flat disk and then spraying it with an acrylic lacquer to form a support for the pressed powder.

The self-supporting Sn^{116} target (95.74% Sn^{116}, 1.02% Sn^{117}, 1.49% Sn^{118}, 1.06% Sn^{120}, and 0.69% other Sn isotopes) was rolled to a thickness of about 5 mg/cm^2 at the UCLRL Machine Shop on a dual-roller press designed for foil production. Stainless steel holders were used to sandwich the tin during the rolling process.

The In^{115} self-supporting target was produced in a manner similar to that used by Frank Grobelch of UCLRL in making the thin beryllium stripper foils for the Hilac (see also Ref. 17). The In^{115} (99.99%) was evaporated in vacuum from a molybdenum boat which was heated by passing a current of $\sim$ 100 amperes through it. The indium vapor was deposited on a 2-in. $\times$ 3-in. glass microscope slide which had previously been coated with a layer of Teepol, a synthetic detergent supplied by Shell Development. After the layer of indium had reached the desired thickness, the heat was removed and the vacuum let up to atmospheric pressure.

The glass slide was then placed in a holder, 30^{o} to the horizontal plane, and water was allowed to slowly lift the foil off the glass slide. The foil was removed from the water by placing the target holder 90^{o} to the water surface, immersing the target holder into the water completely, making contact with the foil with the top of the target holder, and slowly reducing the height of the water. This allows the target holder to act as the support for the foil, and mounting the foil at the same time.

(Since indium is classified with a moderate to high toxic hazard rating,[18] proper precautions must be observed in handling it.)

2. Radiochemical Study of Pr^{134} Decay

In studying the energy levels of Ce^{134}, radiochemical separation and study of the radioactive decay of Pr^{134} were employed as well as the "in-beam" technique. The procedure was similar to that used by Chanda.[7]

The target of copper iodide was prepared by evaporating the copper iodide in vacuum and depositing it on 2.7 mg/cm^2 nickel foil. Target thickness varied from 1-2 mg/cm^2.

A beam of carbon ions, with a beam current of around 150 mμA, was used. The praseodymium nuclei produced were chemically separated from the other products present. A crude excitation function was measured, and Pr^{134} was produced with maximum yield by selecting the beam energy as $\sim$ 90 MeV.

The carbon ion beam passed into the target chamber through a 7.1 mg/cm^2 nickel vacuum foil and through absorber foils before hitting the target.

(The target chamber was the same as used in Ref. 7.) A total of ten weighted aluminum absorbers were available to degrade the beam. The range-energy curves of Northclift[19] were used to select the proper absorber foil to give the desired beam energy.

The recoil atoms were stopped in aluminum catcher foils which could be removed from the target chamber, and the chemical procedure to separate the products started within thirty seconds.

The beam was stopped in a Faraday cup which also monitored the intensity of the beam.

The aluminum catcher foil was dissolved in 10 M sodium hydroxide, and Fe^{3+} carrier was added to bring down the praseodymium as the hydroxide. The $Fe(OH)_3$ was dissolved with concentrated hydrochloric acid and removed with the use of a Dowex-1 anion column eluted with 6 M HCl. The separation of the carrier-free praseodymium from the other rare-earth elements was accomplished with the use of Dowex-50 cation-exchange resin eluted with 0.53 M α-hydroxy isobutyrate[20] buffered to pH = 4.5. The Dowex column had previously been calibrated by the use of Ce^{141} and Ce^{144} tracers and was monitored with a solid-state detector placed at the tip of the column to indicate the activity of each drop as it was formed and fell into numbered sample cones. The signals from the detector were amplified and fed to a chart-recorder where visual observation of the activity could be accomplished.

Since the above procedure took from 30-40 minutes, the following more rapid chemical procedure was also used. The aluminum catcher foil

was dissolved in a 3-ml lusteroid cone with 10 M sodium hydroxide and Ce^{3+}, Pr^{3+}, and Ba^{2+} carriers added. This brings down the praseodymium activities as hydroxides which were then washed with hot water. After dissolving the precipitate with concentrated nitric acid, the sodium hydroxide was again added to precipitate the hydroxide; hot water is used to wash it, and it is again dissolved in concentrated nitric acid. Hot concentrated hydrofluoric acid was added which brings down the praseodymium fluoride. The precipitate was washed with dilute hydrofluoric acid and was considered ready for counting. This procedure was accomplished in at least 5 minutes, and the spectrum obtained was identical to that obtained using the column procedure. Since the bombardments were kept to around 15 minutes in length and the cerium and lanthanum nuclei in the region have long half lives, very little activity other than that from the praseodymium was produced in the rare-earth region. This accounts for the lack of other rare earth activities which would have followed the above chemical separation. Targets of copper and nickel were used to check for other activities which might also follow the chemical separation; these targets showed little if any activity after chemical separation, and none in the region of interest.

The counting of the sample was accomplished using a 3-in. × 3-in. diameter NaI(Tl) crystal mounted to a DuMont 6363 photomultiplier tube.[21] A Victoreen 400-channel pulse-height analyzer was used to collect and display the spectra.

B. Instrumental Methods

1. "In-Beam" Gamma-Ray Detection

The gamma-ray detection system is shown in simple block diagram in Fig. 2. The spectra were taken using a 2 × 3 cm lithium-drifted germanium detector with a depletion layer of ~ 6 mm. The detector bias voltage was 900 volts, supplied by an ORTEC Detector Control Unit. The resolution of the Ge detector was 6.1 keV for Co^{60}.

The germanium detector was placed 90° to the beam, and at an angle of 45° to the target (Fig. 3). In order to minimize stray capacitance and noise, the preamplifier for the detector was connected directly to the signal lead from the detector, through sintered glass, sealed with epoxy resin. Figure 4 shows the germanium counter assembly with the low-noise preamplifier attached, the liquid nitrogen "chicken feeder" (Linde CR-10 Cold Trap Reservoir), and the Varian Associates Varion pump which was used to maintain a pressure of around 5×10^{-6} mm Hg inside the detection system.

Modular TranLamp amplifiers (LRL Drawing 15 × 4845) were used throughout most of this work. The signal was amplified in the single delay line mode, and sent to the RIDL 400-channel Model 34-12B analyzers, and a Tektronix 541A oscilloscope. By observing the counting rate and baseline shift on the oscilloscope due to the counting rate, beam currents were selected to minimize gain shifts and resolution effects due to high counting rates.

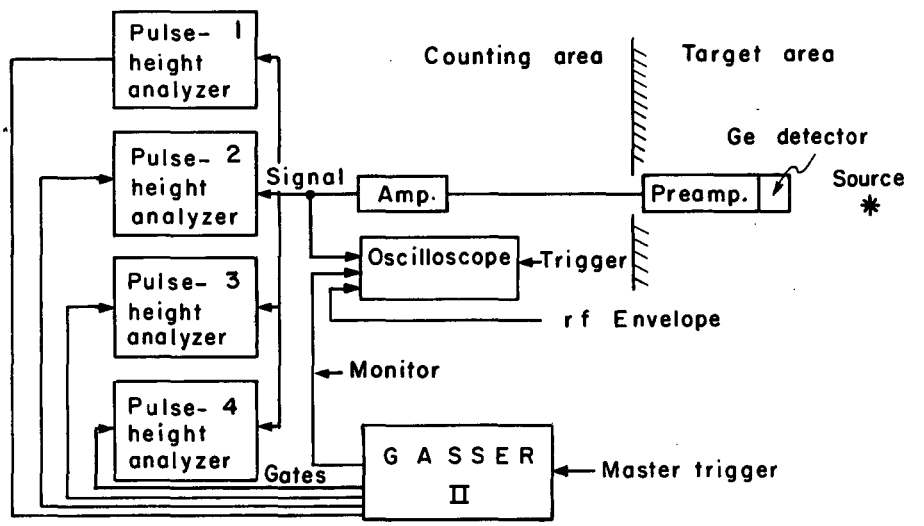

Fig. 2. Simplified block-diagram of the electronics used in the gamma-ray measurements.

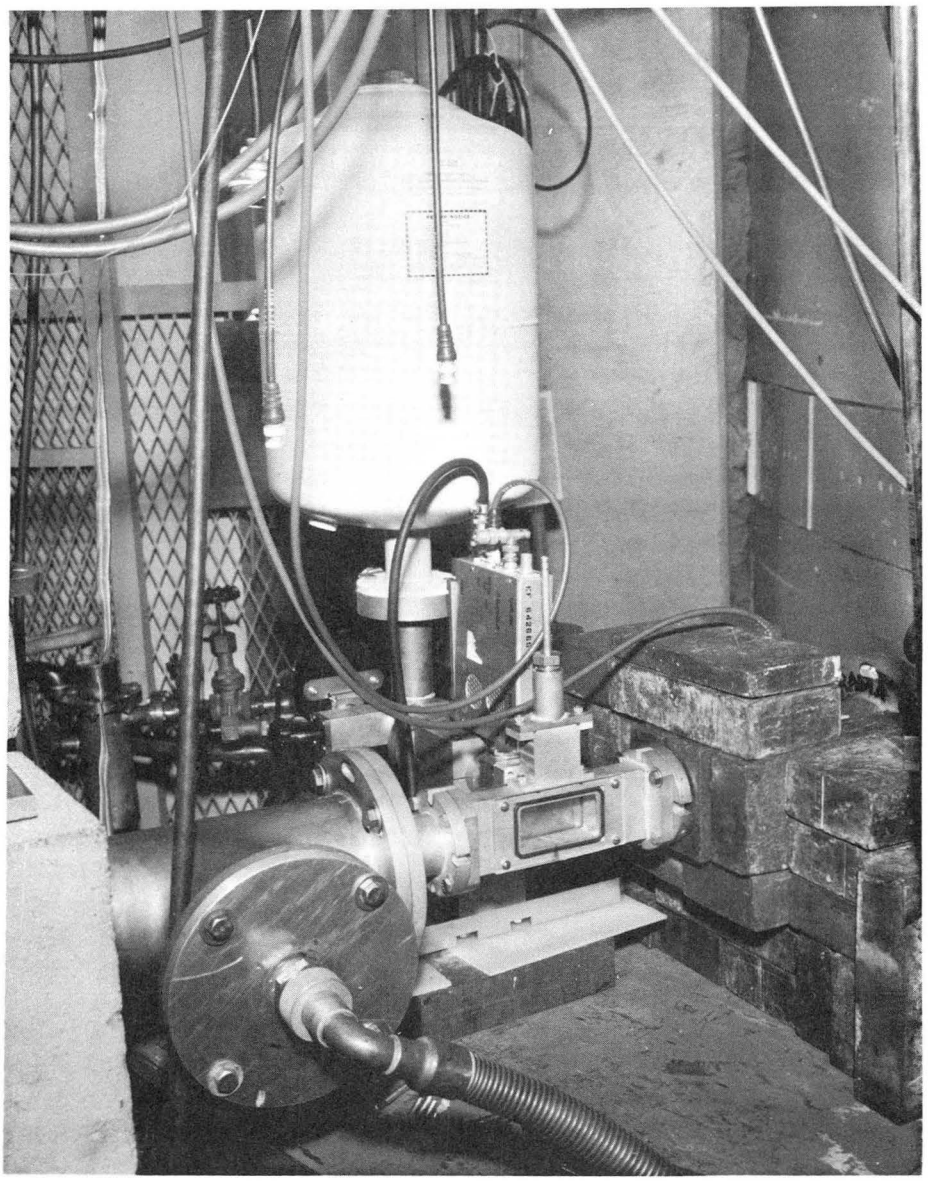

ZN-5018

Fig. 3. Photograph of the germanium detector, target holder arrangement used for the gamma-ray measurements.

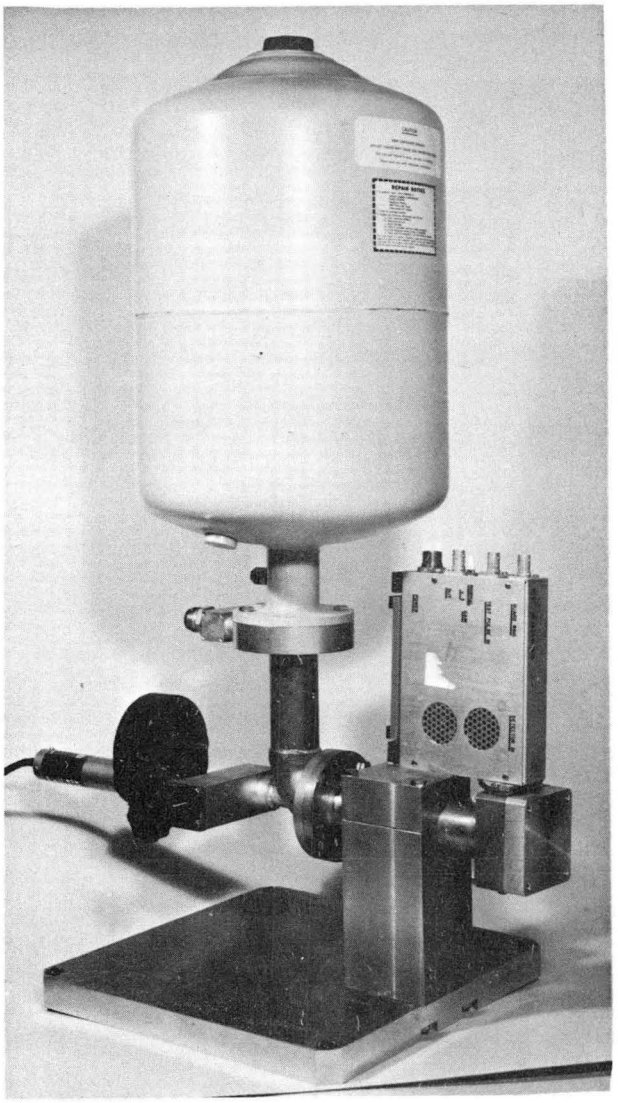

ZN-5019

Fig. 4. Photograph of the germanium detector assembly.

In order to count only during the beam bursts, means of gating the RIDL analyzers on a time basis was designed by Richard G. Leres of UCLRL. The unit, called a Gating and Sequential Subgrouping External Router (GASSER)[22] was used to provide the time sequence gating needed with the analyzers. A total of twelve gates, individually variable from several microseconds to two seconds, were available. The gates can be triggered independently or in a sequential manner.

The timing-pulse arrangement of GASSER can be seen by referring to Fig. 6 which illustrates the various gates and pulses used in connection with the electron spectrometer in measuring the lifetime of the first-excited state of Ba^{126}. The employment of these gates is discussed with the lifetime apparatus. The Hilac master trigger was used to start the sequential operation of GASSER II, a modification of the original GASSER.

2. Lifetime Measurement Procedure

The method used for measuring the lifetime of the first-excited state of Ba^{126} was essentially that of Novakov, Hollander, and Graham.[14] The equipment was set up by Burde, Diamond, and Stephens.

The diagram of the high-voltage target arrangement is shown in Fig. 5. As the reaction products are made, they are given a recoil energy around 5 MeV. Depending on the mean lifetime of the level, conversion electrons are given off before they reach the negative high-voltage grid. The electrons are then slowed down by the negative-voltage gradient depending on the distance from the grid. After passing the grid, the electrons are accelerated by the full-voltage gradient to an energy

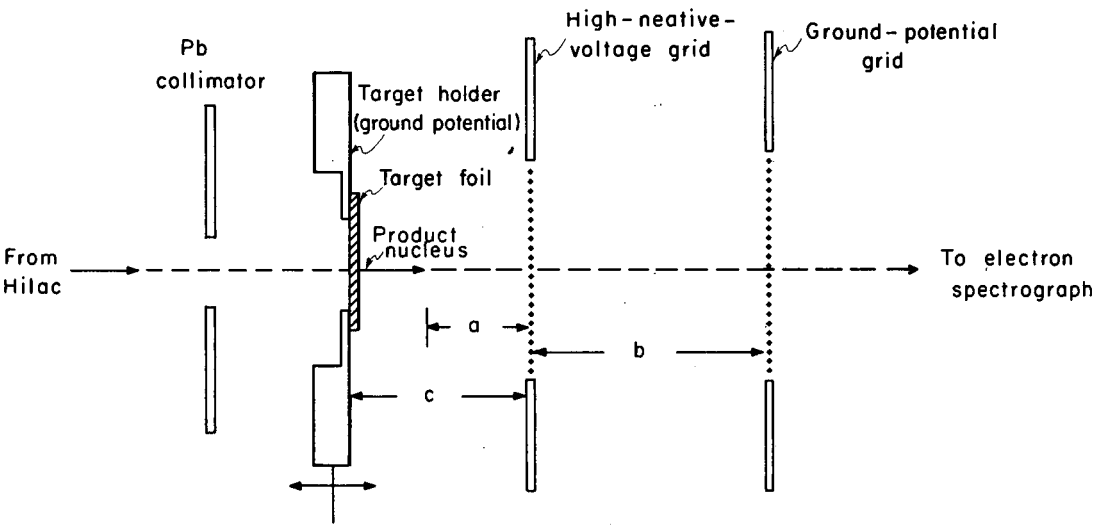

Fig. 5. Drawing of the target-high voltage assembly used to measure the lifetime of the first-excited state of Ba^{126}. The distance c could be varied over limits, while the distance b was fixed.

greater than their original energy. In this manner an electron is given an additional amount of energy, the magnitude of which depends on the recoil distance before electron emission, and therefore, the lifetime of the nuclear state involved. By comparing the electron energy with the high voltage off to that when it is on, and with a knowledge of the recoil velocity and electric field magnitude, a value of the mean lifetime of the state can be obtained.

The recoiling atom leaves the target foil and travels in the direction of the spectrometer with velocity v_r. Assuming that the recoil velocity of the product is not altered by the decay of the compound nucleus, the recoil energy of the final product is given by:

$$E_r = E_b A_b A_r / (A_b + A_t)^2 \qquad (1)$$

where A_b, A_r, and A_t are the mass number of the bombarding particle, b; the recoil atom, r; and the target, t. The energy calculated in this manner is used to obtain the velocity of the recoil atom;

$$v_r = (2E_r/M)^{1/2}(f) \qquad (2)$$

where M is the mass of the recoil atom, and f is a factor which allows for the slowing down of the recoil in the target.

In estimating f, and with a target thickness of $\sim 200\ \mu g/cm^2$, the average thickness seen by a recoil atom would be approximately $100\ \mu g/cm^2$. Assuming that the range of the recoil atom is proportional to its energy,[23,24] this would reduce the energy of the recoil to $0.6\ E_r$. Since the velocity depends on the square root of the energy, the velocity of the recoil atom

would only decrease to 0.8 of the original velocity. This sets f as 0.8 for the targets used in the present work.

The distance traveled after the recoil atom leaves the target and before emission of the conversion electron is

$$D = v_r t \quad , \tag{3}$$

where t is the time involved.

The electron energy as it passes the high negative voltage grid is:

$$E_g = E_i - (1 - \frac{D}{c})V_o e \quad , \tag{4}$$

where E_i is the initial electron energy, e is the electronic charge, V_o is the applied voltage, and c is the distance from the target to the grid. The electron is then accelerated by the negative voltage gradient and receives an energy change $V_o e$. The final energy of the electron when leaving the last grid is:

$$E_f = E_i - (1 - \frac{D}{c})V_o e + V_o e = E_i + \frac{D}{c} V_o e \tag{5}$$

or:

$$E_f = E_i + \frac{D}{c} V_o \text{ (electron volts)} \tag{6}$$

$$\Delta = E_f - E_i \quad . \tag{7}$$

Using the energy of the peak of the electron distribution as found by the electron spectrometer with and without the high voltage applied, the value of Δ can be found,

$$\Delta = kd \tag{8}$$

where k is the energy/channel setting of the electron spectrometer and

d is the channel difference in the electron peak energy distribution as found. Using this relationship,

$$D = \frac{\Delta}{(V_o/c)} \tag{9}$$

and

$$t = \frac{\Delta}{(V_o/c)v_r} \cong \tau \tag{10}$$

where τ is the mean lifetime of the state.

The single wedge-gap type electron spectrometer used to analyze the electrons and its automatic operation has been previously described.[25] The signal from the spectrometer was amplified and sent to the analyzer where it was gated by the pulse sent from GASSER II.

GASSER II timing pulse arrangement is shown in Fig. 6. The Hilac master trigger started Gate 1 which was used as a delay gate to trigger the high voltage pulse during alternate beam pulses. Gate 2 was triggered by Gate 1 also, and was used as a delaying gate to allow the leading edge of Gate 3 to be set to coincide with the beginning of the flat portion of the rf envelope representing the beam pulse. The following edge of Gate 3 was adjusted to end with the beam burst. Gate 3 was used to gate the signal from the electron spectrometer using the first 100 channels of a 400-channel RIDL analyzer.

Gates 4 and 5 were set to monitor "out-of-beam" activity and were used to gate the second and third 100 channels of the analyzer. Gate 6 was not used. Gate 7 was triggered by the alternate Hilac master trigger of that which triggered Gate 1, and was used as a delaying gate to adjust

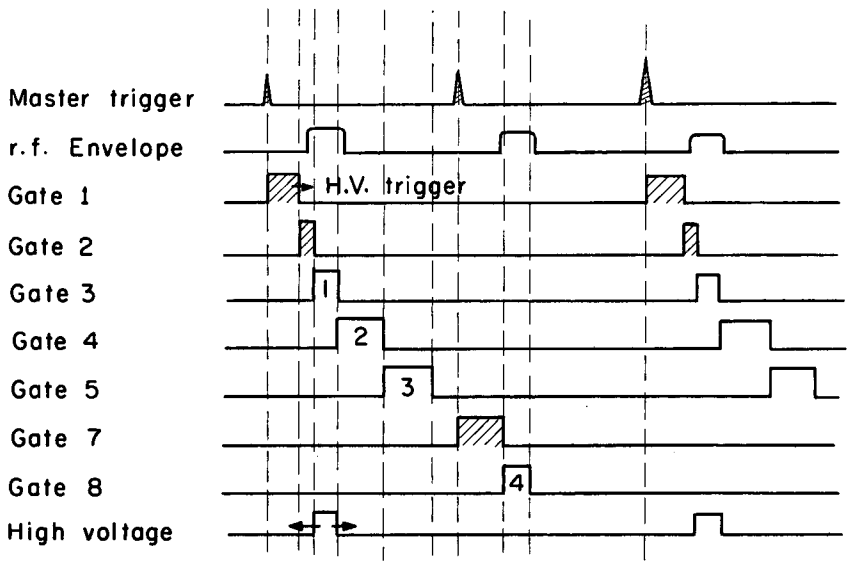

Fig. 6. The timing-pulse arrangement of GASSER II for the life-time determination. (See text.)

the leading edge of Gate 8 to coincide with the beginning of the rf envelope flat portion. The following edge of Gate 8 was set to end with the end of the flat portion of the rf envelope. This gate was used to gate the fourth 100 channels of the analyzer.

The spectrum resulting from the first 100 channels of the analyzer was the electron energy distribution as influenced by the high negative voltage, while the spectrum of the fourth 100 channels represented the distribution with the high voltage off.

III. ISOTOPE RESULTS

The mass assignments of the nuclei considered in this work were based on several criteria. The peak of the calculated excitation function for a product formed in a "x neutrons out" reaction was used as a starting point for investigation of the nuclides studied. (In all cases the assignments were consistent with these predictions.) The assignment of the gamma-rays from Ba^{126} and Xe^{122} was facilitated by comparison with the values previously found by Chanda[6] (Ba^{126}) and Morinaga and Lark[26] (Xe^{122}). The results of the Pr^{134} radiochemical study and the "in-beam" method both support the assignment of the Ce^{134} levels. Since Ba^{124} was produced by two reactions, with different targets and projectiles, both in agreement, the mass assignment is considered to be quite certain.

The spin and parity assignments were made from the systematics of the expected rotational bands. These include (1) the way the energies fit the centrifugal stretching treatment (see Sec. IV), and (2) the observation that in all cases when the spins and parities were known, the ground-state rotational band was the most prominent (or only) band populated by the method used. In the case of Ba^{126}, the lowest energy transition was shown to be E2 from its K/L intensity ratio.

The germanium counter was calibrated by the use of several gamma-ray standards. The Lu^{177m} standard used in the 0-500 keV range is an exceptionally good standard for the Ge counters since it has over 20 transitions or peaks easily resolved with these counters.[27,28] The use of Lu^{177m} and other standards enabled us to measure the gamma-ray energies to an accuracy of $\pm$ 0.3%.

In the following, the properties of the different nuclides will be discussed individually. Section IIIF will summarize the data, and discuss the nuclei more fully.

A. Barium-126

The gamma-ray spectra as found near the peak of the $In^{115}(N^{14}, 3n)$ excitation function is shown in Fig. 7. The relative intensities of the first four transitions of Ba^{126} as observed were 1.00:0.65:0.47:0.26 (after correction for absorbers and detector efficiency). In addition to the transitions that have been assigned to Ba^{126}, three other peaks were found. The 511-keV annihilation radiation peak, the 560-keV In^{115} coulomb excitation peak, and a 690-keV peak can be seen. The 690-keV peak, which is observed in all the Li-drifted germanium counter spectra where neutrons are present, is assumed to result from a $Ge^{72}(n, n')Ge^{72*}$ reaction. The Ge^{72} is excited to the 690-keV 0+ level which then de-excited by electron conversion to the 0+ ground state. Since the electrons are emitted within the germanium crystal, they are captured and detected with very high efficiency as the 690-keV peak.

In comparison with Fig. 7, the gamma-ray singles spectrum[7] from the decay of La^{126} ($t_{1/2} \sim 1$ minute) is shown in Fig. 8. The purpose of showing this figure is very apparent. The ease and precision with which Fig. 7 allows the assignment and energy of the transitions to be made can be contrasted with the difficulty encountered by Chanda. The radiochemical study required gamma-gamma coincidence measurements and still left an amount of uncertainty. In spite of this, the difference in the transitions

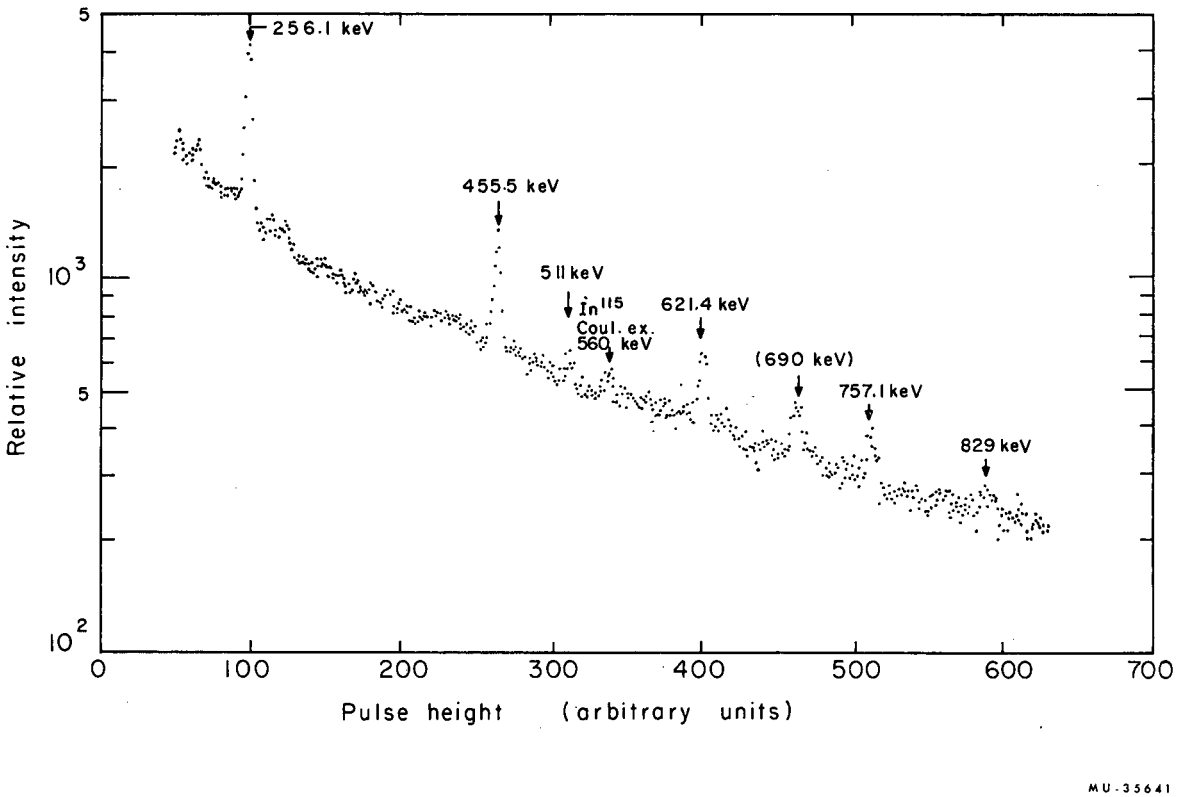

Fig. 7. Pulse-height spectrum as observed for In^{155} target bombarded by 52 MeV N^{14} ions.

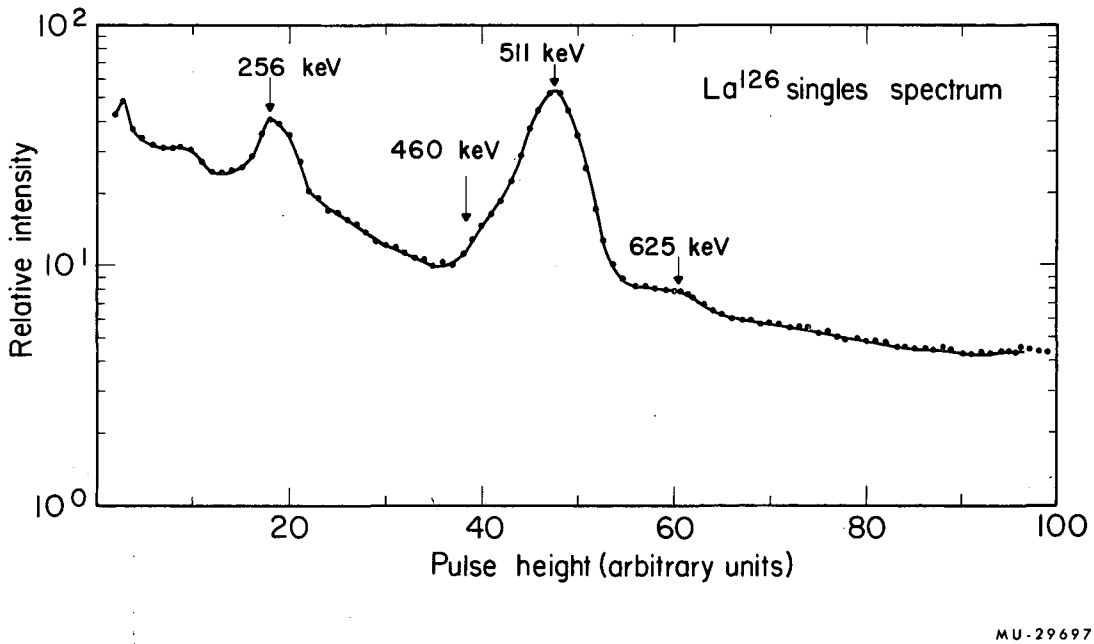

Fig. 8. La^{126} gamma ray singles spectrum for the energy range 0-1000 keV. This figure is taken from Chanda et al., ref. 6.

energies as found by Chanda and those of this work are less than one percent.

The partial-level scheme involving the ground-state rotational band is shown in Fig. 9.

The K/L ratio of the 256-keV level was 4.5 ± 0.6, and while agreement with the theoretical value[29] for an E2 transition is not exact (K/L = 5.4), the transition has been assigned as an E2 transition. The K/L (theoretical) for an M1 transition of this energy would be 7.5.

An example of the electron spectra observed in the lifetime study of the first-excited state of Ba^{126} is shown in Fig. 10. The mean lifetime (τ) for the 256-keV transition was $2.7 \pm 0.5 \times 10^{-10}$ seconds. The limits of error quoted are due mainly to the statistical uncertainty in the calculation of the centroid peaks of the electron distribution. (In determining the lifetime of the 2+ level, an approximate value for the 455-keV 4+ transition was also measured. This value, 8×10^{-11} seconds, has been subtracted from the $2 \rightarrow 0$ lifetime to allow for the effect of the decay from the $4 \rightarrow 2$ level.) Figure 11 shows the value for the 256-keV transition along with other values in various regions. This figure follows that of Grodzins.[30] The value for the lifetime as determined above gives a deformation (β) of Ba^{126} of 0.24 ± 0.02, using Eqs. (25 - 27). β is the deformation parameter of a spheroid given by $\beta = 4/3(\pi/5)^{1/2}(\Delta R/R_o)$ with R_o the mean nuclear radius and ΔR the difference between the major and minor semi-axis of the spheroid.

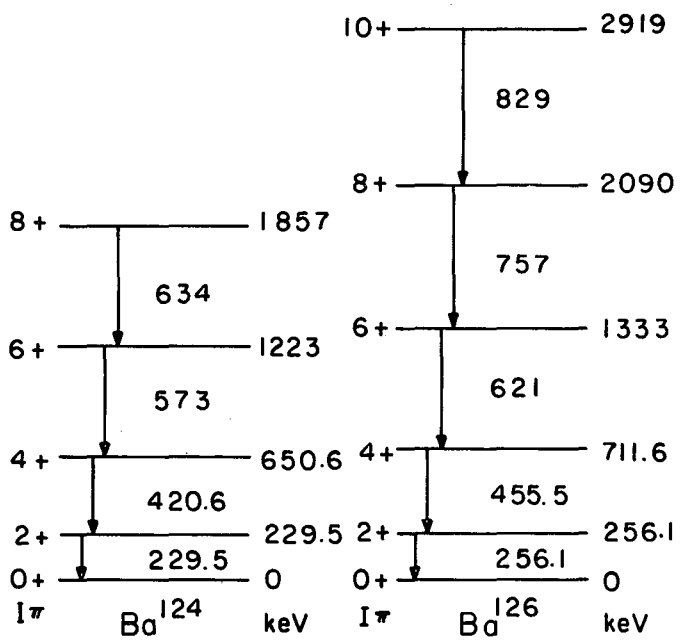

Fig. 9. The partial level scheme of barium isotopes as found in this work.

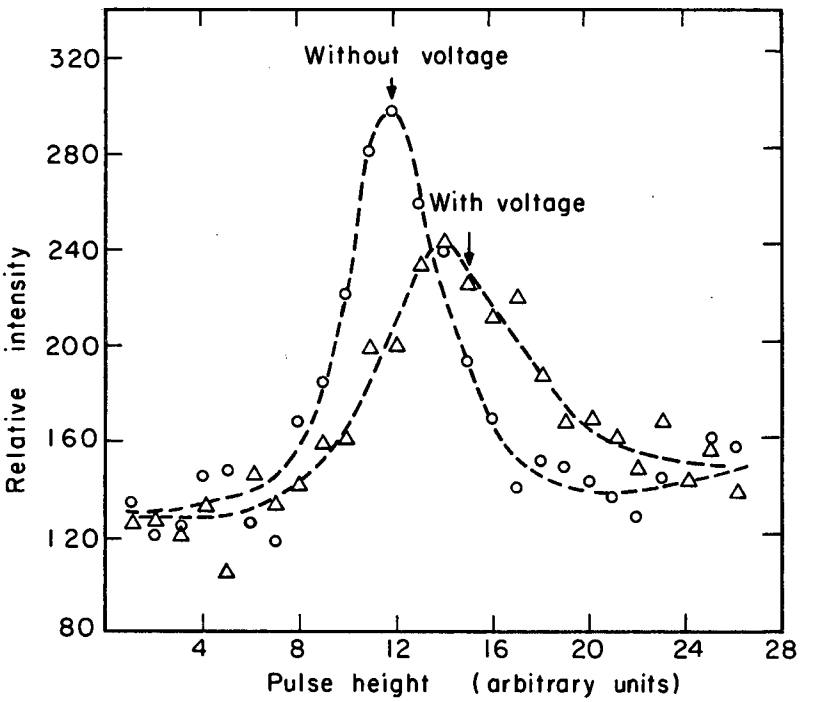

Fig. 10. The electron spectra resulting from an In^{115} target bombarded with 52 MeV N^{14} as found using the lifetime apparatus.

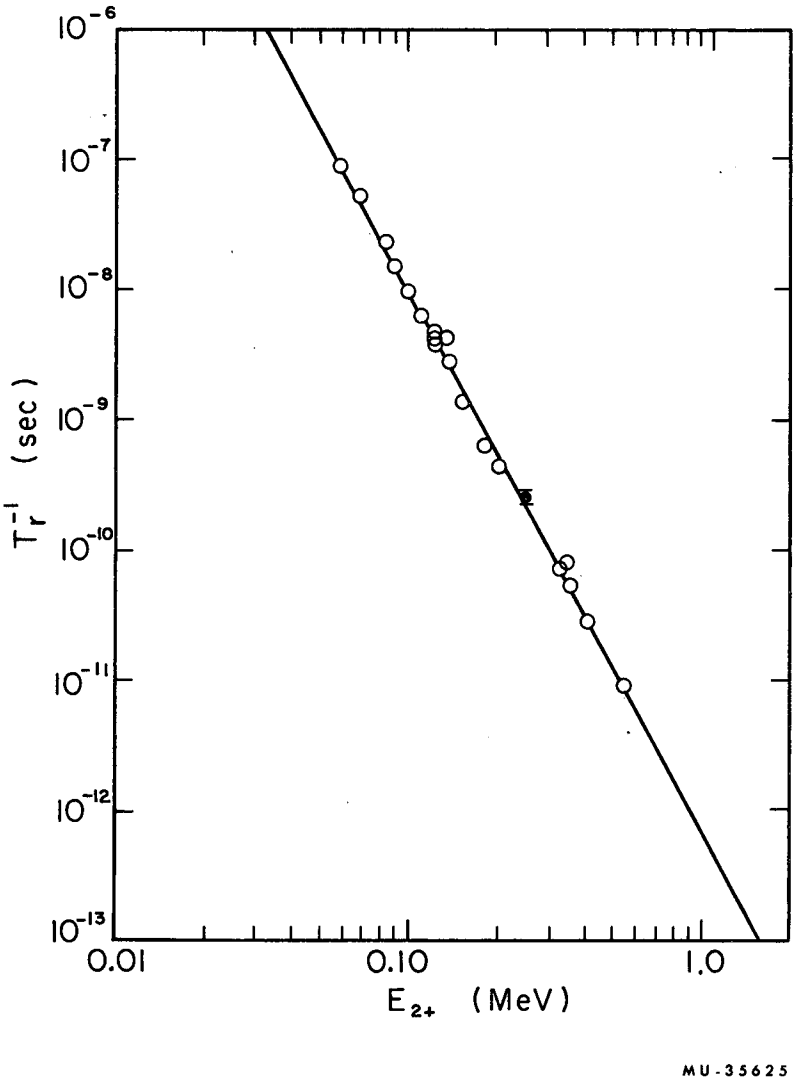

Fig. 11. Reciprocal transition probability T_γ^{-1} $(2 \rightarrow 0) = \tau_\gamma$ as a function of energy, E_{2+}. The solid point represents the value determined in the present work. The open circle values are from Ref. 30.

B. Barium-124

Of the five nuclei considered in this work, Ba^{124} has the least reliable assignments of gamma rays in its decay. Since Ba^{124} was produced in $In^{115}(N^{14}, 5n)$ and $Sn^{116}(C^{12}, 4n)$ reactions, the background is much higher as compared with Ba^{126} which was formed in $In^{115}(N^{14}, 3n)$ reaction. The peaks of Ba^{124} occur at higher bombarding energies where more reactions are possible. The products from these reactions all contribute to the background. Of these products, those formed in $(N^{14}, \alpha xn)$ and $(C^{12}, \alpha xn)$ reactions may become useful in future study of this region.

The 229-keV gamma ray was assigned as the $2 \rightarrow 0$ transition of Ba^{124}. As can be seen in the $Sn^{116}(C^{12}, 4n)$ spectra shown in Fig. 12, there is also a prominent 189-keV peak in the spectra. This peak was also present in the $In^{115}(N^{14}, 5n)$ reaction. It appears to follow the excitation function with the other peaks which have been identified as Ba^{124} transitions, although this determination was crude enough to leave some question. However, from a preliminary lifetime measurement, the 189-keV lifetime appeared to be about an order of magnitude longer than the 229-keV transition and unreasonably long for a collective E2 transition of this energy. On the basis of this and the systematic variation of the energies of the first-excited states of the barium nuclei, the 229-keV transition was assigned as the $2 \rightarrow 0$ transition. It is hoped that future investigation on this nuclide will allow placement of the 189-keV transition.

Figure 9 gives the partial-energy level diagram for Ba^{124}.

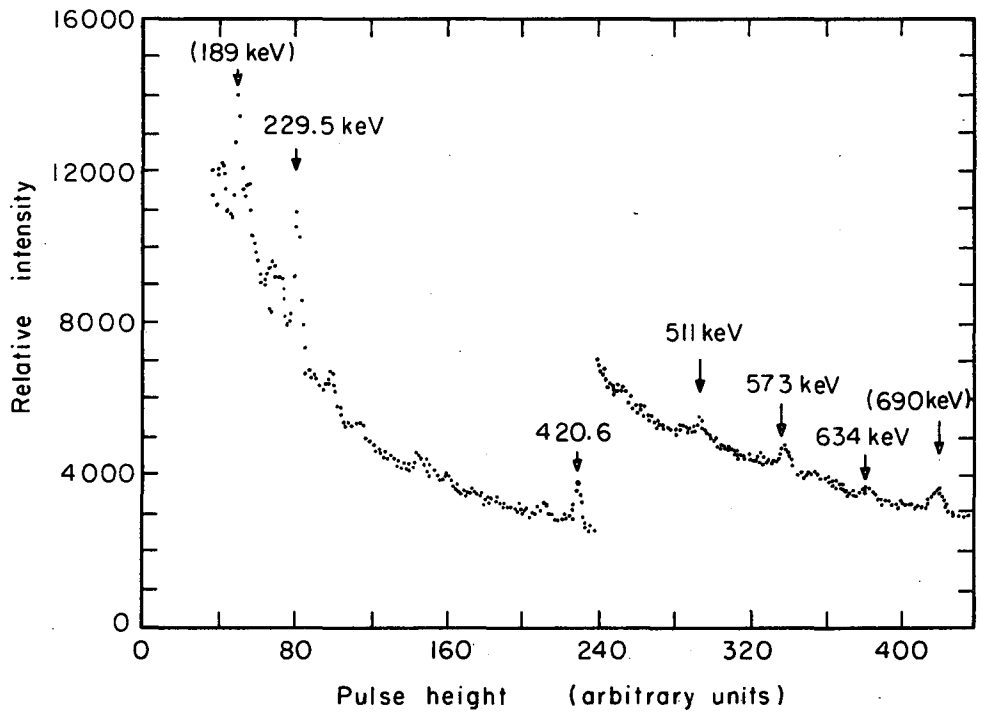

Fig. 12. Pulse-height spectrum as observed for a Sn^{116} target bombarded with 80 MeV C^{12} ions.

C. Xenon-122

The spectra as found in the $In^{115}(B^{11}, 4n)$ reaction is shown in Fig. 13. While the background for this reaction is higher than the $In^{115}(B^{10}, 3n)$ reaction, the peaks found are essentially the same. The five transitions identified with Xe^{122} are the most prominent; however, there is a peak at 460 keV which did not follow the same excitation function as the other peaks. This peak seems to be due to Xe^{123}, and did not appear in the $(B^{10}, 3n)$ reaction to any extent. For $In^{115}(B^{11}, 4n)$ the 819-keV assignment is complicated by several peaks (see Fig. 13); assignment was made by comparing the $In^{115}(B^{10}, 3n)$ peaks. The relative intensities of the first four transitions, after correction for absorbers and counter efficiency was 1.00:0.87:0.86:0.74 in Xe^{122}.

Morinaga and Lark[26] also studied the levels of Xe^{122} using the $Te^{122}(\alpha, 4n)$ reaction and NaI(Tl) counters. The agreement of the two works is very good. (See Table II.)

The partial-level decay scheme as determined by the present work is shown in Fig. 14.

D. Xenon-120

The first three ground-state rotational band transitions found in the $In^{115}(B^{10}, 5n)Xe^{120}$ reaction were assigned without ambiguity (Fig. 15). They are very prominent and easily identified by their excitation functions and systematic spacing. The next two peaks in the band were not assigned, however, with the same assurance. The 690-keV neutron-induced peak is present, and there also appears to be another peak at 701 keV.

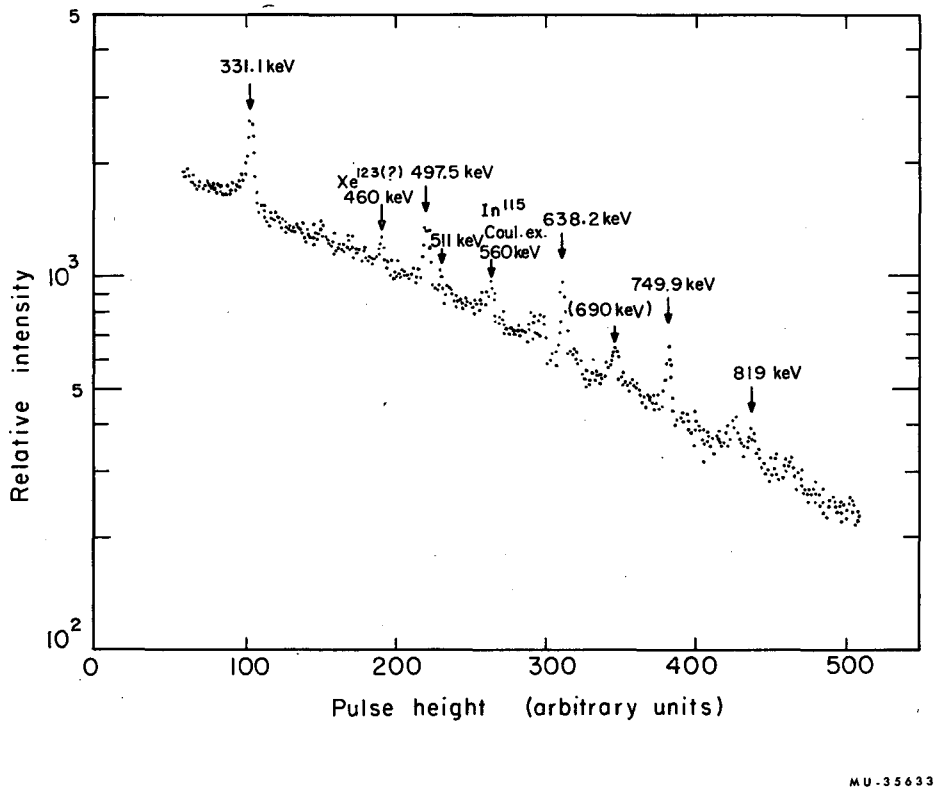

Fig. 13. Pulse-height spectrum as observed for an In^{115} target bombarded with 57 MeV B^{11} ions.

Table II. Ground-state rotational band transition energies of Xe^{122} (keV).

Transition	This work	Morinaga and Lark[26]
$2 \rightarrow 0$	331.1	337
$4 \rightarrow 2$	497.5	502
$6 \rightarrow 4$	638.2	640
$8 \rightarrow 6$	750	750
$10 \rightarrow 8$	$\sim$ 819	$\sim$ 830

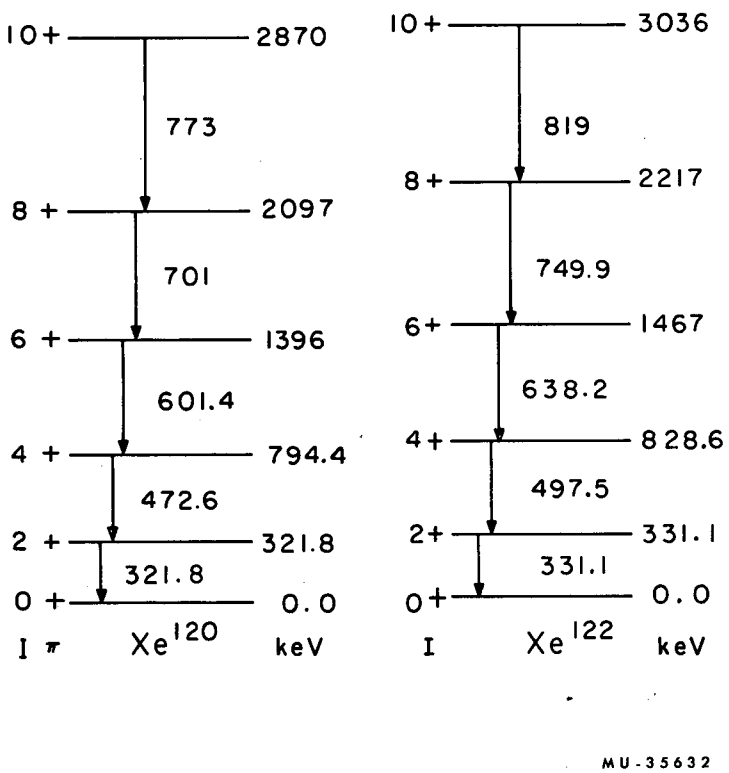

Fig. 14. The partial level scheme of xenon isotopes as found in this work.

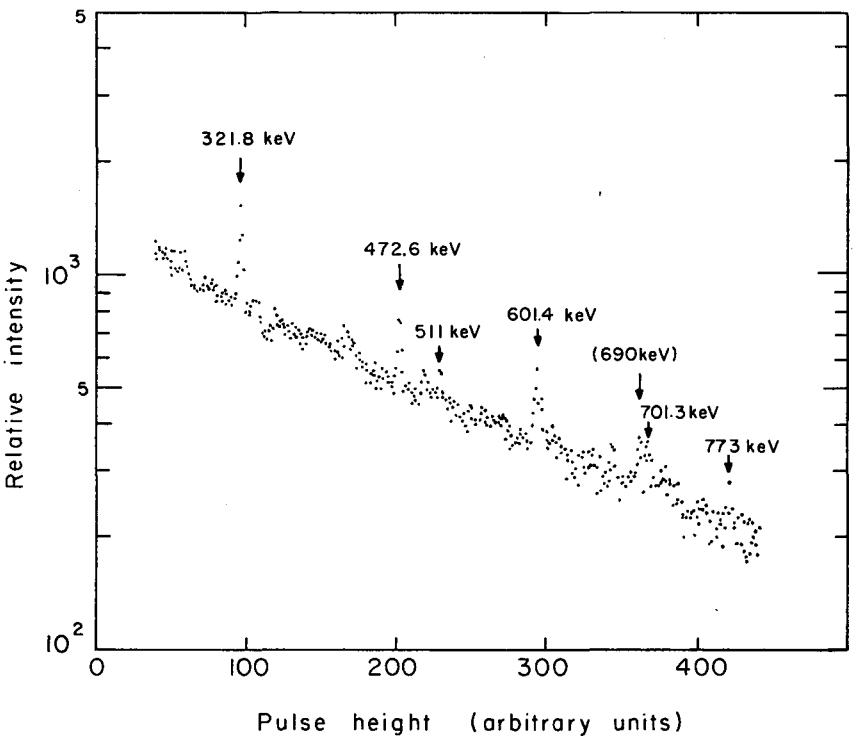

Fig. 15. Pulse-height spectrum as observed for an In^{115} target bombarded with 67 MeV B^{10} ions.

There is also evidence for a peak at 773 keV. The 701-keV and 773-keV peaks have been tentatively identified as the 8 → 6 and the 10 → 8 transitions respectively in Xe^{120}.

The partial-energy level scheme for Xe^{120} is shown in Fig. 14.

E. Praseodymium-134, Cerium-134

The gamma-ray spectrum associated with the decay of Pr^{134} is shown in Fig. 16. Also present in this spectrum are gamma rays from the decay of $Pr^{135} \xrightarrow{\beta,EC} Ce^{135}$, as evidenced by the 220-keV and 300-keV peaks. The 410-keV peak was assigned as the 2 → 0 transition and the 635-keV transition as the 4 → 2 in Ce^{134}.

The placement of the 960-keV peak is uncertain. It is possible that it represents the 2' → 0 gamma-band transition. Using the systematics for the vibrational levels as proposed by Simons,[31] the E_{2+} (K = 2) predicted would be 942 keV. Since very little information is known for vibrational levels in this region, however, the peak was not assigned. Since only the 2 → 0 and 4 → 2 transitions are possibly the 2' → 0 transition were seen in any appreciable amount, the spin of the parent Pr^{134} activity is probably quite low.

The observation of the decay of the 410-keV gamma ray resulted in a half life for Pr^{134} of 17 ± 2 minutes. Since there are relatively few sources of error in the determination of half life by γ decay other than those involved in background subtraction, this result is held to be more accurate than the value of $t_{1/2} \sim 1$ hour obtained in bombardments of samarium with 660-MeV protons.[32]

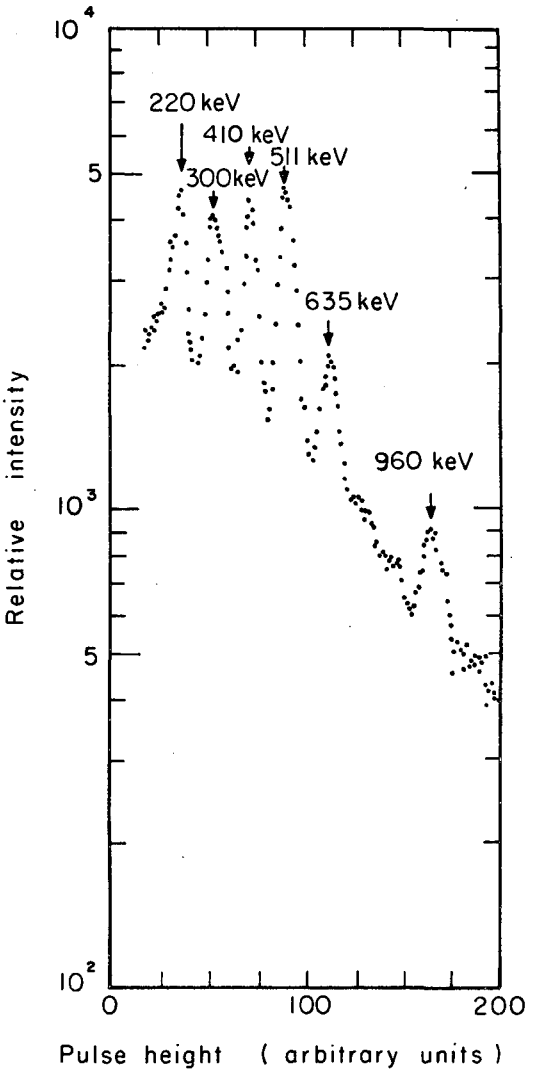

Fig. 16. Pr^{134} gamma-ray spectrum. The Pr^{134} was produced by the $I^{127}(C^{12}, 5n)$ reaction.

The spectra obtained with the "in-beam" technique in the $I^{127}(B^{11}, 4n)$ reaction is shown in Fig. 17. The $I^{127}(B^{10}, 3n)$ reaction was also investigated but the coulomb excitation of I^{127} dominated the spectrum at the energies necessary for the 3n reaction.

The assignment of the first two peaks agrees well with the radiochemical experiment. The 815-keV peak has been assigned as the $6 \rightarrow 4$ transition. The 871-keV peak was tentatively assigned as the $8 \rightarrow 6$ transition, while the peak at 840 keV was not assigned. The 871-keV peak was chosen on the basis of the systematic spacings involved.

Figure 18 shows the partial-energy level scheme for Ce^{134}.

F. Summary and Implications of Results

A summary of the ground-state rotational band transitions as determined in this work is shown in Table III. The classification system of the transition used has the following designation: A, definite peak, definite assignment; B, definite peak, rather indefinite assignment; and C, indefinite peak and indefinite assignment. The nuclei studied in this work are all at the edge of a region of deformation, and hence the transitions and deformation determined in this work are of interest in extending the knowledge of nuclear shapes in this region.

In stating the evidence for a new region of deformation with less than 82 neutrons, Chanda[6,7] used several methods to estimate the deformation of the barium nuclei from the energy levels involved. Three of these methods have been considered in the following: (1) the comparison of the first-excited state energies E_{2+} with an $(E_{2+})_{crit}$ as suggested by Alder

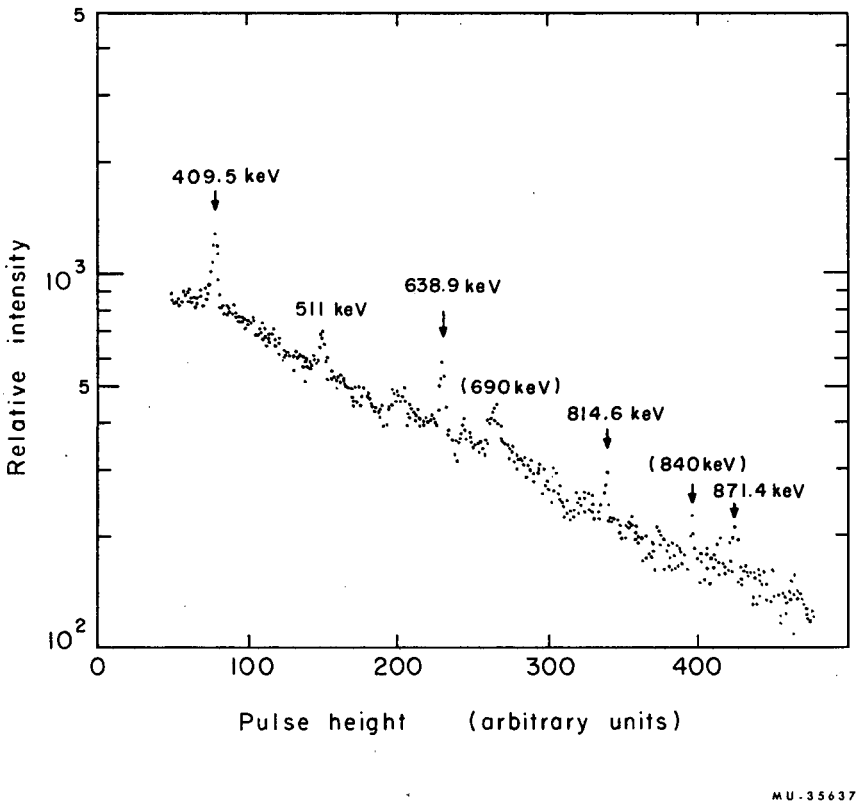

Fig. 17. Pulse-height spectrum as observed for an I^{127} target bombarded with 57 MeV B^{11} ions.

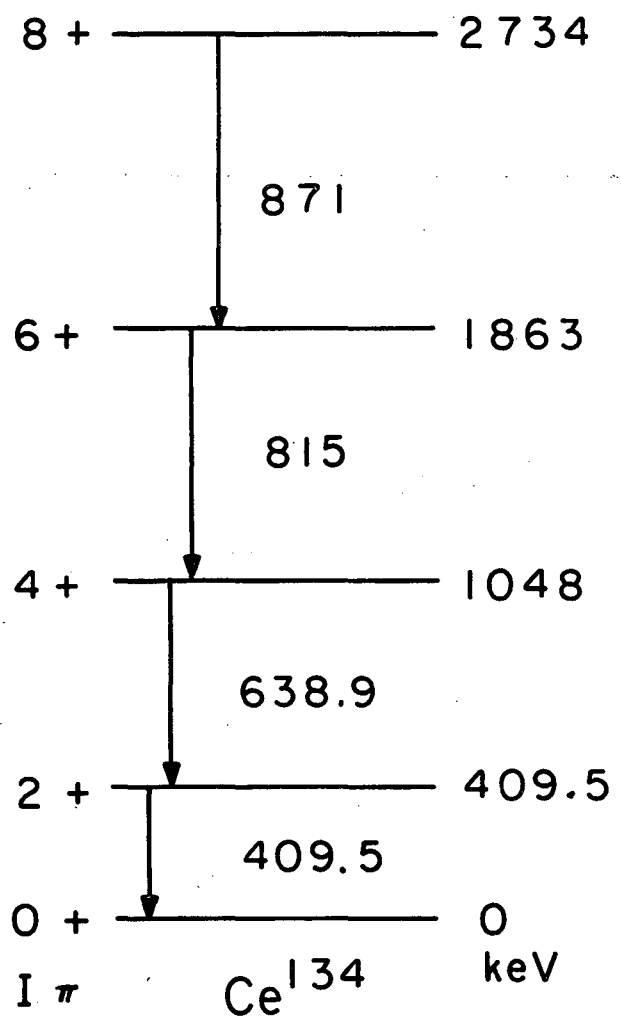

Fig. 18. Partial level scheme for Ce^{134}.

Table III. Ground-state rotational band transitions* (keV).

Transition	Xe^{120}	Xe^{122}	Ba^{124}	Ba^{126}	Ce^{134}
2 → 0	321.8 A	331.1 A	229.5 A	256.1 A	409.5 A
4 → 2	472.6 A	497.5 A	420.6 A	455.5 A	638.9 A
6 → 4	601.4 A	638.2 A	573 B	621.4 A	814.6 A
8 → 6	701 C	749.9 A	634 B	757.1 A	871.4 B
10 → 8	773 C	819 C		829 B	

*The accuracy of these transitions is expected to be ± 0.3%. The additional significant figure used in most cases is of interest only in comparing transitions of similar energy in the same nucleus.

et al.,[33] (2) the collective-model description of Bohr and Mottelson,[3] and (3) the theoretical calculations of Marshalek, Person, and Sheline.[34] In addition to the above considerations, the values of deformation as calculated by Myers and Swiatecki[35] from their mass formula are included. (Section IV of this work utilizes the concept of centrifugal stretching in a treatment of the nuclei in this work and those in Ref. 10.)

The energy of the first-excited state of the even-even xenon, barium, and cerium isotopes is shown in Fig. 19. To obtain an estimate of the transition between rotational and vibrational nuclei, the value of the first-excited state is compared to a critical value[33] given by:

$$(E_{2+})_{crit} = \frac{3\hbar^2}{0.23\,\mathcal{S}_{rig}} \qquad (11)$$

where $\mathcal{S}_{rig}$ is the moment of inertia of a rigid rotator as given in Eq. (33) of Sec. IV. Since no dependence upon Z is included in the evaluation of $(E_{2+})_{crit}$, there is some uncertainty as to the applicability of this model. If $E_{2+} < (E_{2+})_{crit}$, the model implies that rotational spectra should occur and the nuclei are considered deformed.

The first-excited states of Ba^{126} and Ba^{124} lie below the value of $(E_{2+})_{crit}$ as can be seen in Fig. 19, and are, therefore, considered deformed nuclei and indicative of a region of deformation.

For even-even nuclei with a ground state of $I = K = 0$, the ground-state rotational-band energy levels are fairly well described using the collective model of Bohr and Mottelson.[3] This model predicts (to first order) the energy levels of deformed nuclei as a function of I given by:

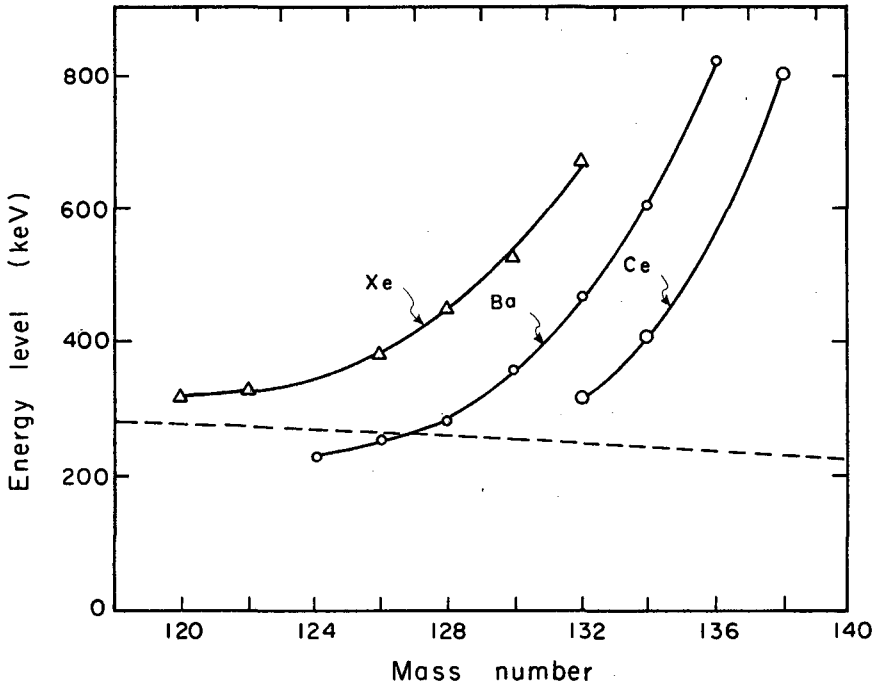

Fig. 19. The energy of the first-excited states of the even-even xenon, barium, and cerium isotopes. The $(E_{2+})_{crit}$ shown as the dashed line indicates the transition between spherical and spheroidal nuclei. (The Ce^{132} point is an approximate value as observed in the I^{127} (C^{12},7n) reaction.

$$E_I = \frac{\hbar^2}{2\Im} I(I+1) \qquad (12)$$

where I represents the spin of the state, and $\Im$ is the moment of inertia, and only even spin states and positive parity are allowed. For a rotational band with spins I = 2, 4, 6, 8, ..., Eq. (12) predicts the energy ratios:

$$E_4/E_2 = 3.33 \quad ; \quad E_6/E_2 = 7.00 \quad ; \quad \text{etc.}$$

Figure 20 shows the energy level ratios E_I/E_2 (ratio of the energy of the state with spin I to the energy of the first-excited 2+ level) for typical nuclei in the various regions and the nuclides of this work. There are several places where the ratio shows a sharp rise, and approaches the limit as calculated above.

The rise in the rare-earth and heavy-element regions are regarded as indication of deformation in these regions. Since a similar rise can be seen for the nuclei just below 82 neutrons, this may also indicate deformation.

As seen in the comparison of E_{2+} with $(E_{2+})_{crit}$ and the ratio E_I/E_{2+}, the more neutron-deficient barium isotopes studied seem to have the largest deformation. The value for the quantity E_I/E_{2+} for Xe^{120}, as determined in this work, is lower than that for Xe^{122} and, therefore, the deformation (or tendency toward deformation) of the xenon isotopes appears to have reached a maximum with Xe^{122}. The more neutron-deficient isotopes of cerium, on the other hand, will probably have still larger deformations, and may well exceed those of the barium isotopes.

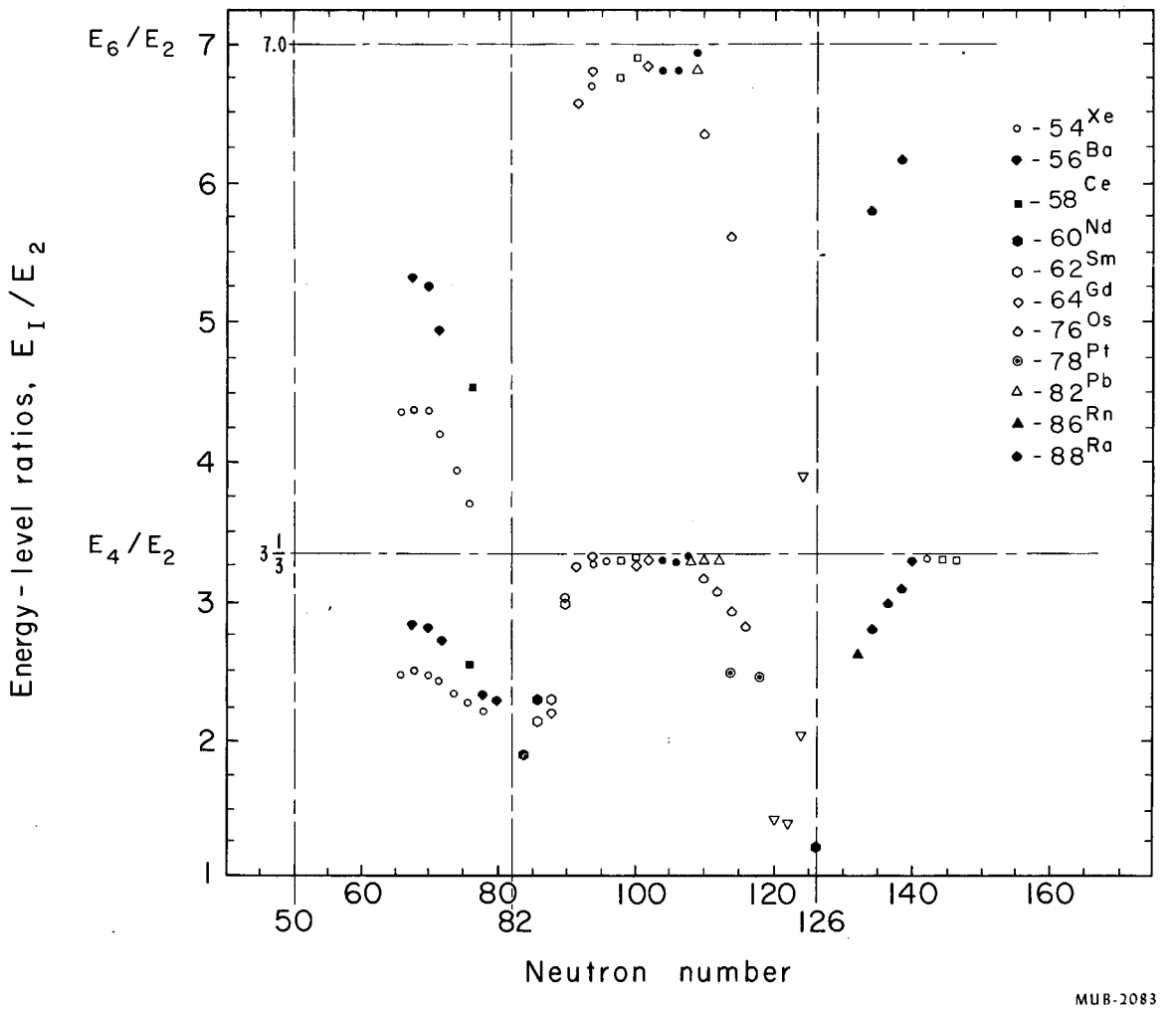

Fig. 20. The energy ratio E_I/E_{2+} of the even-even nuclei represented. The neutron closed-shells are indicated by the vertical dashed lines; the Bohr-Mottelson theoretical limits are shown as horizontal dashed lines. The data has been given in Ref. 7.

The experimental value of β for Ba^{126} as determined from the lifetime of the first-excited state [see Eq. (28) etc.] is compared with calculated values of Marshalek et al.[34] and Myers and Swiatecki[35] (see Fig. 21). Marshalek et al. summed the Nilsson single-particle energies, without pairing force or Coulomb corrections, as a function of deformation and obtained a value for the total nuclear energy. The deformation shown corresponds to the value of deformation for which the energy summation was a minimum.

The Myers and Swiatecki values are obtained as a result of the semi-empirical mass-formula calculations, and are based on the potential energy surface given for the nuclei involved.[35]

The agreement of the experimental points of the present work and those of Fagg[36] with the calculations of Myers and Swiatecki is very good. The major difference between the values from the two theoretical works seems to be more of magnitude in the deformation rather than if deformation exists. Both treatments agree as to the variation of deformation with mass number; although the magnitude seems thus far to be fit better in this region by Myers and Swiatecki.

The lifetime as determined in this work for the first state in Ba^{126} can also be used to indicate the deformation of the region by calculating the enhancement factor, F, for this transition. The enhancement factor is:

$$F = \frac{T_\gamma(\text{experimental})}{T_\gamma(\text{s.p.},\ 2 \rightarrow 0)} \qquad (13)$$

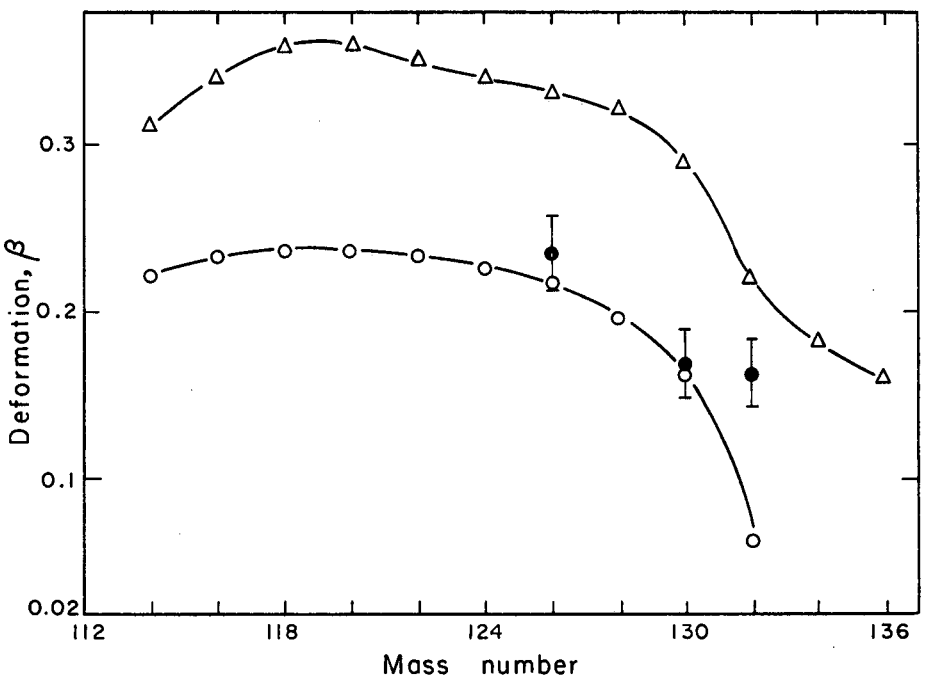

Fig. 21. Deformation, β, for the even-even barium nuclides. The Δ represent the values of Marshalek et al.,[34] and the o indicate the Myers and Swiatecki[35] values. $Ba^{130,132}$ deformations are from Fagg.[36]

where the single proton transition probability, T_γ, is given by:[30]

$$T_\gamma(\text{s.p.},\ 2 \rightarrow 0) = 7.5 \times 10^7\ E_\gamma(2 \rightarrow 0)A^{4/3} \qquad (14)$$

with $E_\gamma(2 \rightarrow 0)$ in MeV, T_γ is in sec^{-1}, A is the mass number, the statistical factor has been set equal to one, and the nuclear radii have been assumed to vary as $r = 1.2\ A^{1/3}$ fm. For the $2 \rightarrow 0$ transition in Ba^{126}, $F \cong 70$, a value which approaches those obtained in the deformed rare-earth and heavy-element nuclei.

It must be pointed out that there appears to be no sharp discontinuity of nuclear properties in this region (such as occurs in regions above the 82 neutron shell) which would indicate the definite onset of deformation. Thus, to make more definite statements concerning nuclear shapes, one would have to know a considerable amount about higher collective (vibrational) excitations. In the absence of such information, we can only compare the ground-state band properties of these nuclei with those of comparable nuclei, lying in regions where more confidence is placed in knowledge about the nuclear shapes. This has been done, and indicates that most likely Ba^{124} and Ba^{126} in particular have stable equilibrium deformations.

IV. CENTRIFUGAL STRETCHING TREATMENT OF NUCLEI

A. General Treatment

Bohr in his considerations of the coupling on nuclear surface oscillations to the motion of individual nucleons[37] proposed the following Hamiltonian:

$$\mathcal{H} = \frac{\hbar^2}{2B}\left[\frac{\partial}{\beta^4\partial\beta}\left(\beta^4\frac{\partial}{\partial\beta}\right) + \frac{1}{\beta^2\sin 3\gamma}\frac{\partial}{\partial\gamma}\left(\sin 3\gamma\frac{\partial}{\partial\gamma}\right) - \frac{1}{4\beta^2}\sum_{k=1}^{3}\frac{L_k^2}{\sin^2(\gamma - 2\pi k/3)}\right] + 1/2\, C\beta^2 \tag{15}$$

where β and γ are deformation parameters, B is a mass parameter, C is a potential energy parameter, L_k is the projection of the nuclear angular momentum on the principle axes, and $4B\beta^2\sin^2(\gamma - 2\pi k/3)$ are the moments of inertia on the principle axes.

This Hamiltonian was used by Davydov and Filippov[38] as a starting point for their treatment of an ellipsoidal nucleus where no interchange of energy with vibrational or intrinsic states during rotation was considered. Their Hamiltonian was:

$$\mathcal{H} = \frac{\hbar^2}{4B\beta^2}\sum_{k=1}^{3}\frac{L_k^2}{2\sin^2(\gamma - 2\pi k/3)} \quad . \tag{16}$$

The energy levels for deformed even-even nuclei using this rigid asymmetric rotor model were calculated by Moore and White.[39]

To extend the asymmetric rotor model, Davydov and Chaban[40] assumed the nucleus was rigid against γ vibrations but not β vibrations. Equation (15) then becomes:

$$\mathcal{H} = \frac{\hbar^2}{2B}\left[\frac{1}{\beta^3}\frac{d}{d\beta}\left(\beta^3\frac{d}{d\beta}\right) - \frac{1}{4\beta^2}\sum_{k=1}^{3}\frac{L_k^2}{\sin^2(\gamma - 2\pi k/3)}\right] + \frac{1}{2}C(\beta - \beta_o)^2 \quad , \quad (17)$$

where the inclusion of β_o as a parameter allows for the possibility of oscillation of the nucleus about a spheroidal instead of a spherical shape. Day, Klema, and Mallmann[41] computed the energy levels of asymmetric even nuclei using the Davydov-Chaban model.

More recently, it was shown that a classical treatment[42] of centrifugal stretching could be used to calculate the rotational levels of the nucleus. For an axial symmetric nucleus, the energy of the nucleus (E_n) consists of a potential energy (P.E.) quadratic in the change of deformation from an equilibrium value similar to the Davydov-Chaban quantum mechanical treatment, and a rotational kinetic energy (K.E.) equal to $\hbar^2 I(I + 1)$ divided by twice the moment of inertia:

$$E_n = \text{P.E.} + \text{K.E.} = 1/2\ C(\beta - \beta_o)^2 + \frac{\hbar^2 I(I + 1)}{2\Im(\beta)} \qquad (18)$$

where $\Im(\beta)$ represents the moment of inertia.

The method used in the present work as a centrifugal stretching treatment of nuclei is essentially that used in the above classical treatment. A better expression for the potential energy in Eq. (18) can be obtained by using the deformation energy constants as derived by Swiatecki:[35]

$$\text{P.E.} = a\beta^2 - b\beta^3 + c\ \exp(-D\beta^2) \qquad (19)$$

where a, b, c, D are constants specified by the mass formula. The values of the mass-formula constants for typical nuclei are given in Table IV,

Table IV. Mass-formula constants for typical nuclei.*

Nucleus	a	b	c	D	c†
Ba^{126}	36.95	8.01	4.47	27.47	4.26
W^{174}	32.48	12.14	6.07	34.08	5.64
U^{238}	25.09	15.49	7.92	41.95	20.4

*Reference 35.

†The fitted value of c taken from the two-parameter C.S.(III) treatment.

along with the fitted value for c which is discussed in Secs. IVB and IVC. Replacing the potential energy part of Eq. (18) with Eq. (19) results in:

$$E_n = a\beta^2 - b\beta^3 + c\exp(-D\beta^2) + \frac{\hbar^2 I(I+1)}{2\Im(\beta)} \quad . \tag{20}$$

The terms of Eq. (20) are shown graphically in Fig. 22, along with E_n for W^{174}, as fitted in a two-parameter calculation (as explained in Sec. IVB). As can be seen from this figure, the minimum in E_n, which represents the equilibrium deformation of the nucleus, moves to higher values of β as the spin of the nucleus increases, as a consequence of centrifugal stretching.

In evaluating the energy of the nucleus [Eq. (20)], the variation of the moment of inertia with deformation must be specified. Three possibilities have been considered.

1. $\Im(\beta) \propto \beta^2$

Using the form of the hydrodynamic model, the relationship of the moment of inertia with changing deformation is:

$$\Im(\beta) = 3B\beta^2 \tag{21}$$

where B is taken as a parameter, rather than the hydrodynamic value. Substituting Eq. (21) into Eq. (20), we have:

$$E_n = a\beta^2 - b\beta^3 + c\exp(-D\beta^2) + \frac{\hbar^2 I(I+1)}{6B\beta^2} \tag{22}$$

and setting $e = \hbar^2/6B$, (23)

$$E_n = a\beta^2 - b\beta^3 + c\exp(-D\beta^2) + eI(I+1)\beta^{-2} \quad . \tag{24}$$

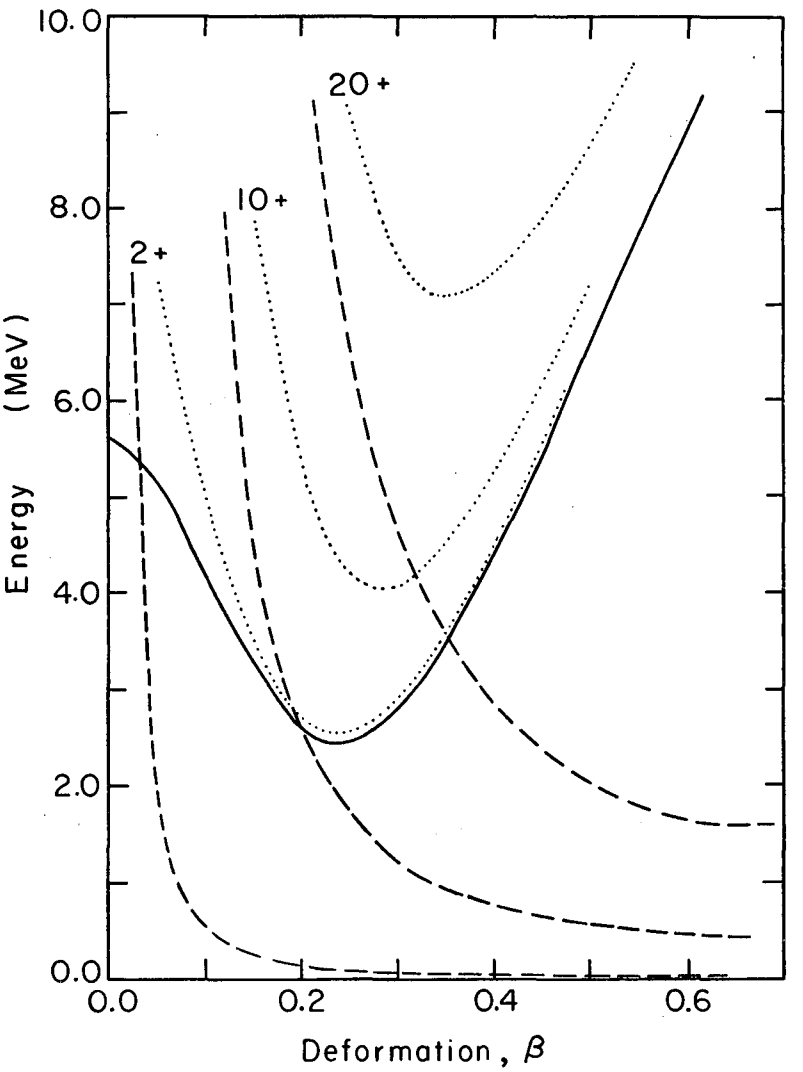

Fig. 22. The dotted line is the nuclear energy, E_n, in Eq. (20) for three values of I; the dashed line represents the kinetic energy term; and the solid line represents the potential energy. The curves are for the parameters of W^{174}.

The designation C.S.(I) will be used in referring to energies calculated using Eq. (24).

To evaluate Eq. (23) for use (1) for zero-parameter estimates, and (2) to check the plausibility of the value of e used, the following derivation was used.

Since:

$$B(E2;\ 0 \rightarrow 2) = 407\ T(E2;\ 2 \rightarrow 0)E_\gamma^{-5} \qquad (25)$$

in units of $e^2 \times 10^{-48}$ cm^4, where $B(E2;\ 0 \rightarrow 2)$ is the reduced transition probability for the $0 \rightarrow 2$ transition, $T(E2;\ 2 \rightarrow 0)$ is the gamma-ray transition probability for the $2 \rightarrow 0$ transition, and E_γ is the energy of the $2 \rightarrow 0$ transition in keV,

$$|Q_o| = [10.05\ B(E2;\ 0 \rightarrow 2)]^{1/2} \qquad (26)$$

where Q_o is the quadrupole moment in units of 10^{-24} cm^2, and:

$$\beta = 3.12[(1 + \frac{59\ Q_o}{ZA^{2/3}})^{1/2} - 1] \qquad (27)$$

where Z is the atomic number, and A is the mass number [Eqs. (25), (26), and (27) are given in Ref. 43], we obtain:

$$\beta = 3.12\{[1 + \frac{3780\ E_\gamma^{-5/2}T(E2;\ 2 \rightarrow 0)^{1/2}}{ZA^{2/3}}]^{1/2} - 1\} \quad . \qquad (28)$$

Using the empirical relationship for the transition probability:[30]

$$T(E2;\ 2 \rightarrow 0) \cong 3 \times 10^{-2}\ E_\gamma^4 Z^2 A^{-1} \qquad (29)$$

where E_γ is in keV, and substituting Eq. (29) into Eq. (28):

$$\beta = 3.12[(1 + 653\ E_\gamma^{-1/2}A^{-7/6})^{1/2} - 1] \quad . \qquad (30)$$

Expanding the square-root part of the expression and neglecting higher-order terms, we obtain:

$$\beta = 1020\, E_\gamma^{-1/2} A^{-7/6} \tag{31}$$

which, after converting from E_γ(keV) to E_γ(MeV) and squaring gives:

$$\beta^2 = 1040\, E_\gamma^{-1} A^{-7/3} \quad . \tag{32}$$

By plotting $\beta^2 A^{7/3}$ vs E_γ^{-1}, the constant in Eq. (32) was determined to be closer to 1200 for the rare-earth region, resulting in:

$$\beta^2 \cong 1200\, E_\gamma^{-1} A^{-7/3} \quad . \tag{33}$$

Using the approximate relationship from Eq. (24),

$$E_I \cong \frac{\hbar^2 I(I+1)}{6B\beta^2} \tag{34}$$

then:

$$E_2 - E_o = E_\gamma = \frac{\hbar^2}{B\beta^2} = 6e\beta^{-2} \tag{35}$$

where e is defined in Eq. (23). Substituting Eq. (35) into Eq. (33) and solving for e gives:

$$e = \frac{200}{A^{7/3}} \tag{36}$$

which can then be used in Eq. (24).

2. $\underline{\Im(\beta) = \Im_{rig}(\beta)[1 - \exp(-\beta^2/f^2)]}$

Since $\Im(\beta) \propto \beta^2$ would continue to increase with increasing β beyond the rigid moment of inertia, the application of C.S.(I) is not valid at large deformations. A dependence of $\Im(\beta)$ which has a parabolic shape at

low deformations and approaches the rigid body moment of inertia at large deformations is given by:

$$\Im(\beta) = \Im_{rig}(\beta)[1 - \exp(-\beta^2/f^2] \qquad (37)$$

where $\Im_{rig}(\beta) = 2/5\ AMR^2(1 + 0.31\ \beta + \ldots)$, AM = nuclear mass, $R = r_o A^{1/3}$, and f = parameter. Substituting Eq. (37) into Eq. (20):

$$E_n = a\beta^2 - b\beta^3 + c\ \exp(-D\beta^2) + \frac{\hbar^2 I(I+1)}{4/5\ AMR^2(1 + 0.31\ \beta)[1 - \exp(-\beta^2/f^2)]} \qquad (38)$$

and substituting:

$$\frac{\hbar^2}{4/5\ AMR^2} = \frac{36.27}{A^{5/3}} = e \qquad (39)$$

$$E_n = a\beta^2 - b\beta^3 + c\ \exp(-D\beta^2) + \frac{eI(I+1)}{(1 + 0.31\ \beta)[1 - \exp(-\beta^2/f^2)]} \qquad (40)$$

referred to as C.S.(II).

3. $\Im(\beta) \propto \beta^2 - \beta^4$

Another form for the moment of inertia which is of interest, since it would seem to lie between the two previous forms, is:

$$\Im(\beta) = 3\ B(\beta^2 - \beta^4) \qquad (41)$$

where B is essentially the same as in Eq. (23).

This form of $\Im(\beta)$ would be parabolic at small deformations and would reach its maximum value at $\beta \sim 0.7$, where it would start to decrease and become invalid. Substituting as before for e and $\Im(\beta)$ in Eq. (20) results in:

$$E_n = a\beta^2 - b\beta^3 + c\ \exp(-D\beta^2) + eI(I+1)/(\beta^2 - \beta^4) \qquad (42)$$

designated C.S.(III).

B. Methods of Calculation

The process of finding the equilibrium deformation of a nucleus for each spin from 0 to 20 for C.S.(I), C.S.(II), and C.S.(III) by a trial-and-error procedure could result in a lifelong project. Fortunately, the development of high speed computers has made this problem almost easy.

To obtain the energy of the nucleus and the related deformation, the expression for E_n is differentiated with respect to β, set equal to zero, and solved for β. This deformation, β_{eq}, is used to calculate E_n for the nucleus for that spin. This process must be repeated for each spin for which E_n is desired, and the results determine the energy E_n as a function of spin I.

In order to evaluate an approximate beta-vibrational energy, and a zero-point correction, the second derivative of E_n was evaluated at β_{eq} to obtain the curvature of the effective potential for each value of I. This curvature was used to obtain the zero-point correction as used with a harmonic oscillator potential:

$$1/2\ \hbar\omega = 1/2(C/B)^{1/2} \qquad (43)$$

where C is the curvature of the potential and B is the mass parameter as previously defined. The zero-point correction is added to E_n to give the total energy, TE, of the nuclear state. These total energies can be used to obtain the transition energies and state energies of the nucleus, and can be compared with the experimental values. The beta-vibrational energy was just twice the zero-point correction, $\hbar\omega$. The IBM 7094 computer at UCLRL was used to evaluate β_{eq}, E_n, TE, and the related values.

Stephens, Lark, and Diamond[10] compared the Davydov-Chaban model, involving two parameters, with their experimental values; Harris[44] did a similar comparison using an expression that resulted from considering higher order corrections to the cranking model, also with two parameters. To compare the centrifugal stretching treatment as outlined here with these calculations, the various C.S. methods were parameterized as two-parameter solutions. The value of c in the mass formula was chosen in all the treatments as a parameter to allow some change in the potential energy. In C.S.(I) and C.S.(III), the value of e was varied and in C.S.(II), f was allowed to vary; thus allowing in each case a parameter in the kinetic energy term.

C. Results of Centrifugal Stretching Treatment

The experimental rotational energies for the isotopes considered in the present work are compared with those calculated from C.S.(II) and C.S.(III) in Table V. [C.S.(I) was in the region of three percent deviation for the nuclei considered.] As can be seen, the agreement is quite good. Since all levels of these nuclides were used, including the less reliable assignments, the percent deviation of one to two percent is understandable. The root-mean square of the percent deviation was calculated as:

$$\text{rms } \% \text{ dev.} = \left(\frac{1}{n} \sum_{I_i}^{I_f} \epsilon^2\right)^{1/2} \qquad (44)$$

where I_i, I_f are the initial and final spin considered, ϵ is the percent deviation of the calculated values compared with the experimental values, and n is the number of levels fit.

Table V. Experimental rotational state energies compared with C.S. calculations* (keV).

Isotope		2+	4+	6+	8+	10+	rms % dev.
Ba^{126}	experimental	256.1	711.6	1333	2090	2919	
	C.S.(II)	252.8	727.9	1345	2072	2890	1.38
	C.S.(III)	250.7	732.3	1355	2074	2865	1.98
Ba^{124}	experimental	229.5	650.6	1223	1857		
	C.S.(II)	229.2	655.0	1209	1867		0.70
	C.S.(III)	227.8	659.8	1214	1852		0.88
Xe^{122}	experimental	331.1	828.6	1467	2217	3036	
	C.S.(II)	328.1	844.2	1475	2202	3014	1.06
	C.S.(III)	324.9	855.6	1492	2201	2966	2.13
Xe^{120}	experimental	321.8	794.4	1396	2088	2861	
	C.S.(II)	320.8	806.6	1400	2086	2857	0.78
	C.S.(III)	315.5	819.5	1420	2086	2804	2.10
Ce^{134}	experimental	409.5	1048	1863	2734		
	C.S.(II)	408.1	1062	1848	2732		0.79
	C.S.(III)	406.1	1065	1850	2721		0.99

*There are two parameters in the various C.S. treatments.

It was of interest to compare the C.S. treatments of this region with other regions. Table VI gives the rotational state energy rms % deviation for the two-parameter fits of nuclei in the rare-earth region. The experimental data and Davydov-Chaban values were taken from Ref. 10. For comparison, the average of the rms % deviation of each model is also listed. As can be seen by this table, the agreement is excellent for all the treatments for the nuclei shown; however, the C.S.(III) treatment, a classical treatment, does seem to be the best in this region.

An idea of the deviations involved as a function of spin can be seen from Fig. 23. Here the average percent deviation for the nine nuclei in Table VI are plotted vs the spin of the state. This average % deviation shows the systematic variation among the nuclei considered. An interesting point is the complete reversal of the deivations in the case of C.S.(I) compared to C.S.(II). This reversal was the reason for proposing C.S.(III) which is intermediate between the two previous forms. Since in the region of interest there is not a great deal of difference between the three models, the reversal of the deviations is quite sensitive to the details of the models.

In an effort to examine the applicability of the C.S. treatments to heavy nuclei, Th^{232} and U^{238} were studied. Table VII shows the errors resulting from the three C.S. treatments for these nuclides; they are certainly well within the experimental error limits. Table VIII shows the comparison of the various calculated properties for these nuclei using C.S.(III) with the experimental values. In addition to the fit of the

Table VI. Rotational state energy rms % deviation for two-parameter fit.

Nucleus[a]	Davydov-Chaban[b]	Harris[c]	Centrifugal (I)	Stretching (II)	Treatment (III)
$W^{172}(7)$	0.27	0.69	0.55	0.86	0.25
$W^{174}(6)$	0.16	0.30	0.38	0.23	0.22
$W^{176}(6)$	0.20	0.46	0.20	0.34	0.15
$Hf^{166}(6)$	1.45	0.59	0.90	0.57	0.69
$Hf^{168}(6)$	0.79	0.26	0.69	0.28	0.51
$Hf^{170}(8)$	0.22	0.76	0.24	0.99	0.12
$Hf^{172}(7)$	0.31	0.46	0.10	0.41	0.11
$Yb^{164}(5)$	0.52	0.14	0.48	0.17	0.37
$Yb^{166}(6)$	0.12	0.20	0.23	0.17	0.12
Average	0.45	0.43	0.45	0.42	0.28

[a] Number in parenthesis indicates the total number of levels fit.

[b] Ref. 10.

[c] Ref. 44.

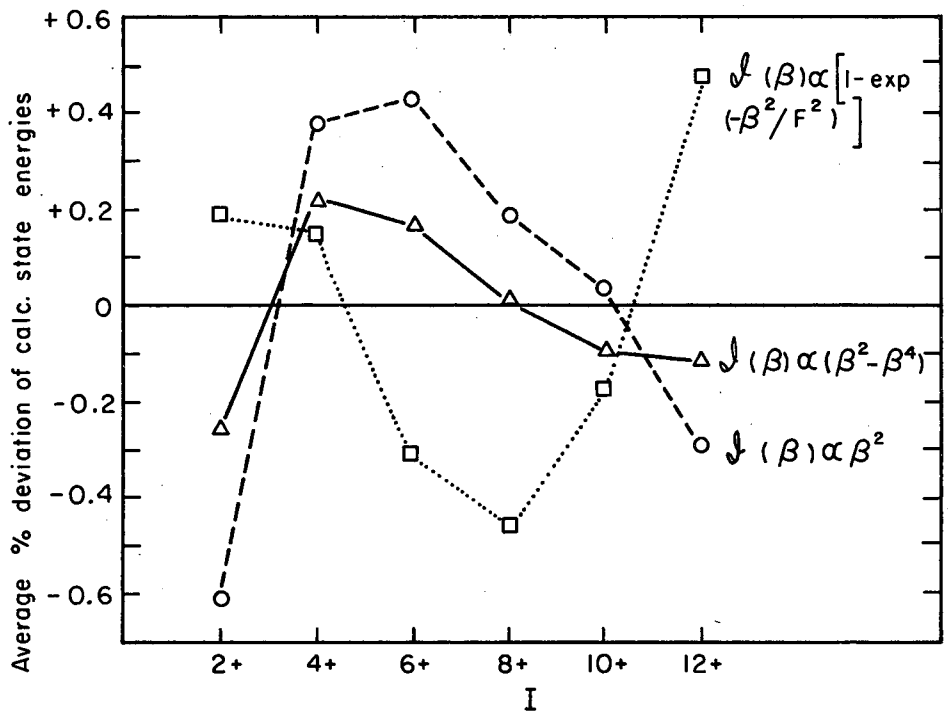

Fig. 23. Average percent deviation of the calculated state energies compared to the experimental values as a function of I, for the three C.S. treatments.

Table VII. Rotational state energy rms % deviation for two-parameter fit.

Nucleus[a]	C.S.(I)	C.S.(II)	C.S.(III)
Hf^{178}(4)	0.017	0.028	0.014
Th^{232}(5)	0.25	0.13	0.22
U^{238}(6)	0.08	0.13	0.08

[a]Number in parenthesis indicates the total number of levels fit.

Table VIII. Experimental values compared with the C.S. calculations.

		Rotational state energies* (keV)						rms % dev.	Calculated $E(0' \rightarrow 0)$ (keV)	Observed $E(0' \rightarrow 0)$[b] (keV)	β_{calc}	β_{obs}[c]
		2+	4+	6+	8+	10+	12+					
Hf^{178}	exp.	93.17	306.9	632.7	1059.7					1197[a]		
	calc.	93.17	306.8	632.7	1059.8	1576.1	2169.3	0.017	1663	1440	0.302	0.265
Th^{232}	exp.	49.75	162.5	334.1	557.9	828.2						
	calc.	49.63	162.9	334.7	558.1	825.9	1131.2	0.22	833	730	0.262	0.257
U^{238}	exp.	44.7	148.2	307.6	518.7	777.0	1078.2					
	calc.	44.8	148.1	307.3	518.6	777.3	1078.4	0.08	1015	993	0.303	0.280

*Th^{232} and U^{238} are from Ref. 45; Hf^{178} data are from the Table of Isotopes. There are two parameters, c and e, in the calculation, using C.S.(III).

[a]Data are less certain.

[b]Ref. 46.

[c]Ref. 47.

rotational energies, the value of the zero-point vibration correction has been used to obtain the values for the $E(0' \rightarrow 0)$ transitions. (Since the form of the zero-point vibrational correction is for harmonic oscillator potentials, not the potential as used in the C.S. treatment, the calculated values are expected to only be approximate.)

Tables VII and VIII also include the same comparisons for Hf^{178} which was selected to study the behavior of the C.S. treatments with good rotors in the rare-earth region. The fit for Hf^{178} is remarkable but in reducing the deviation to such a low value, the parameters used in the two-parameter fit of C.S.(III) were somewhat unrealistic.

The "in-beam" use of electron spectrometers and germanium counters in obtaining experimental transition energies is creating, as demonstrated here and in the other "in-beam" works mentioned, a rapid increase in information on collective (especially rotational) energy levels. This information will certainly be useful in testing various proposed collective models and the centrifugal stretching treatments as proposed here.

The results of the centrifugal stretching demonstrate the ability of a classical treatment to reproduce the experimental rotational state energies. In addition to giving this information, the deformation of the nucleus and an approximate value for the $E(0' \rightarrow 0)$ beta band transition can be calculated and these compare reasonably well with experiment in the few cases thus far tried.

These calculations represent the first attempt to employ realistic nuclear potentials in centrifugal stretching calculations. It is clear

that a number of improvements ought to be made. One should, for example, require fitting of the equilibrium deformation and beta-vibrational energies where these are known. Also the gamma-vibrational band, which is completely absent from this treatment, ought to be taken into account in some way. Nevertheless, the present calculations have been shown to be rather successful in reproducing the experimental data even without these improvements.

V. CONCLUSIONS

The "in-beam" method was used to measure the transition energies of nuclides at the edge of a region of deformation. The ability of this method in giving this information for nuclides with short half-lives has been compared to the more standard radiochemical techniques and was shown to be particularly valuable for collective excitation studies. The lifetime of Ba^{126} as measured indicates a definite deformation for this nucleus.

The systematics of the first-excited state energies of these nuclei along with the rotational band energy spacings have been shown to also indicate deformation in this region.

The calculated deformations of Myers and Swiatecki[35] appear to show good agreement with the several values experimentally determined. As more nuclides are investigated in the future and their deformation determined, the theoretical values can be more intensively compared for this region.

The centrifugal stretching treatment can definitely be considered as an excellent method for calculating energy levels in nuclides although more investigation will be necessary before the systematic nature of the parameters varied can be used for complete prediction of the levels.

ACKNOWLEDGMENTS

I would like to thank my research director, Professor Isadore Perlman for his helpful assistance, advice, and patience in this work.

I also would like to express my deep gratitude to Dr. Richard M. Diamond and Dr. Frank S. Stephens for their aid, encouragement, suggestions, and friendship; to Dr. Jacob Burde for his advice and efforts with the lifetime apparatus.

Special thanks must be mentioned to Dr. Torbjørn Sikkeland for his constant encouragement and frequent discussions concerning this work and the world in general, and to Dr. Richard N. Chanda for his interest and friendship.

In addition, I would like to express my appreciation to Mr. Albert Ghiorso for his interest in this work and aid in scheduling bombardments at times of extreme need; to Mrs. Roberta Garrett for her assistance; to Mr. A. E. "Bud" Larsh for his willingness to help and assist in those electronic problems which arise in moments of stress; to Mr. Richard Leres for his help and design of GASSER and his trouble shooting of other related problems; and to Mr. David Leppaluoto for his writing of the computer programs utilized in the centrifugal stretching computations.

For assistance above and beyond the call of duty, I would like to acknowledge the help of Mr. Frank Grobelch, Mr. Charles Corum, Mr. James Johnston, Mr. Bill Gagnon, Mr. William Stahl, and Mr. William Burgess, and to the many members of the Hilac operating crew for their dedication and ability in providing the necessary conditions for this operation.

To my wife, Edna, whose patience and dedication has aided in the completion of this research, I would like to express my special thanks and devotion.

This work was performed under the auspices of the U. S. Atomic Energy Commission.

REFERENCES

1. R. K. Sheline, Rev. Mod. Phys. 32, 1 (1960).

2. E. Eichler, Rev. Mod. Phys. 36, 809 (1964).

3. A. Bohr and B. Mottelson, Kgl. Danske Videnskab. Selskab, Mat.-Fys. Medd. 27, No. 16 (1953)(edition 2, 1957).

4. J. P. Davidson, Rev. Mod. Phys. 37, 105 (1965).

5. R. K. Sheline, T. Sikkeland, and R. N. Chanda, Phys. Rev. Letters 7, 446 (1961).

6. R. Chanda, J. Clarkson, and R. K. Sheline in Proceedings of the Third Conference on Reactions Between Complex Nuclei, Asilomar, California, April 1963 (University of California Press, Berkeley, 1963).

7. R. N. Chanda, Evidence for a New Region of Deformation With Less Than 82 Neutrons (Ph. D. Thesis), Lawrence Radiation Laboratory Report UCRL-10798, 1963 (unpublished).

8. H. Morinaga, P. C. Gugelot, Nucl. Phys. 46, 210 (1963).

9. G. B. Hansen, B. Elbek, K. A. Hagemann, and W. F. Hornyak, Nucl. Phys. 47, 529 (1963).

10. F. S. Stephens, N. L. Lark, and R. M. Diamond, Nucl. Phys. 63, 82 (1965).

11. K. Miyano, M. Ishihara, Y. Shida, H. Morinaga, T. Kuroyanagi, and T. Tamura, Nucl. Phys. 61, 25 (1965).

12. N. L. Lark and H. Morinaga, Nucl. Phys. 63, 466 (1965).

13. M. Sakai, T. Yamazaki, and H. Ejiri, Physics Letters 12, 29 (1964).

14. T. Novakov, J. M. Hollander, and R. L. Graham, Nucl. Instr. and Methods 26, 189 (1964).

15. J. D. Jackson, Can. J. Phys. 34, 767 (1956). For further details concerning the Jackson Model calculations in a recent application see: C. F. Smith, Jr., Decay of the Zn^{64*} Compound Nucleus Formed by Nuclear Reactions of p, He^3, He^4, and C^{12} with Cu^{63}; Ni^{61}, Ni^{60}, and Cr^{52}, Respectively (Ph.D. Thesis), Lawrence Radiation Laboratory Report UCRL-11862, January 1965 (unpublished).

16. E. L. Hubbard et al., Rev. Sci. Instr. 32, 621 (1961).

17. M. A. Williamson, Preparation of Some Backed and Unbacked Heavy-Element Targets, Lawrence Radiation Laboratory Report UCRL-6989, June 1963.

18. N. I. Sax, Dangerous Properties of Industrial Materials, 2nd Ed. (Reinhold Publishing Corp., New York, 1963).

19. L. C. Northcliffe, Ann. Rev. Nucl. Sci. 13, 67 (1963); NAS-NRC Series, Report No. 8.

20. S. G. Thompson, B. G. Harvey, G. R. Choppin, and G. T. Seaborg, J. Am. Chem. Soc. 76, 6229 (1954).

21. The crystals and photomultipliers were obtained as integral units from Harshaw Chemical Company, Cleveland, Ohio.

22. R. G. Leres, Subgrouping Multichannel Analyzers on a Periodic Basis, Lawrence Radiation Laboratory Report UCRL-11828, January 1965 (Nuclear Chemistry Division Annual Report, 1964).

23. N. Bohr, Kgl. Danske Videnskab. Selskab, Mat.-Fys. Medd. 18, No. 8 (1948).

24. K. O. Nielsen, Electromagnetically Enriched Isotopes and Mass Spectrometry (Butterworth and Co., London, 1956).

25. R. M. Diamond, B. Elbek, and F. S. Stephens, Nucl. Phys. 43, 560 (1963).

26. H. Morinaga and N. Lark, private communication from N. Lark (Raymond College, Stockton, California).

27. P. Alexander, F. Boehm, and E. Kankeleit, Phys. Rev. 133, B284 (1964).

28. D. A. Shirley, Nucleonics 23, No. 3, 62 (1965).

29. L. A. Sliv and I. M. Band, Tables of Internal Conversion Coefficients, in Alpha, Beta, and Gamma-Ray Spectroscopy, Vol. 2, K. Siegbahn, Ed. (North Holland Publishing Co., Amsterdam, 1965).

30. L. Grodzins, Physics Letters 2, 88 (1962).

31. L. Simons, Soc. Sci. Fennics Commentationes Phy.-Math. 25 (7), 13 (1961).

32. A. K. Lavrukhina, G. M. Kolesov, and Tan Syao-en, Izvest. Akad. Nauk S.S.S.R., Ser. Fiz. 24, 1113 (1960).

33. K. Alder, A. Bohr, T. Huus, B. Mottelson, and A. Winter, Rev. Mod. Phys. 28, 432 (1956).

34. E. Marshalek, L. W. Person, and R. K. Sheline, Rev. Mod. Phys. 35, 108 (1963).

35. W. Myers and W. J. Swiatecki, unpublished work, 1965. See also W. J. Swiatecki, Second International Conference on Nuclidic Masses, Vienna, 1963, and W. Myers and W. J. Swiatecki, Nuclear Masses and Deformation, Lawrence Radiation Laboratory Report (in preparation).

36. L. W. Fagg, Phys. Rev. 109, 100 (1958).

37. A. Bohr, Kgl. Danske Videnskab. Selskab, Mat.-Fys. Medd. 26, No. 14 (1952).

38. A. Davydov and G. Filippov, Nucl. Phys. 8, 237 (1958).

39. R. B. Moore and W. White, Can. J. Phys. 38, 1149 (1960).

40. A. S. Davydov and A. A. Chaban, Nucl. Phys. 20, 499 (1960).

41. P. P. Day, E. O. Klema, and C. A. Mallmann, Tables of Energy Levels of Asymmetric Even Nuclei with Beta Vibration-Rotation Interaction, Argonne National Laboratory Report ANL-6220, November 1960.

42. R. M. Diamond, F. S. Stephens, and W. J. Swiatecki, Physics Letters 11, 315 (1964).

43. R. E. Bell, S. Bjørnholm, and J. C. Severiens, Kgl. Danske Videnskab. Selskab, Mat.-Fys. Medd. 32, No. 12 (1960).

44. S. M. Harris, Phys. Rev. Letters 13, 663 (1964).

45. F. S. Stephens and R. M. Diamond, private communication, University of California, Lawrence Radiation Laboratory, Berkeley, California.

46. F. S. Stephens, B. Elbek, and R. M. Diamond, Paper E-8, Proceedings of the Third Conference on Reactions Between Complex Nuclei (University of California Press, Berkeley, 1963); see also F. S. Stephens, N. Lark, R. M. Diamond, Phys. Rev. Letters 12, 225 (1964).

47. B. Elbek, Nuclear Transition Probabilities (Ejnar Munksgaard Forlag, Copenhagen, 1963).